AD-A115 474 COLORADO STATE UNIV FORT COLLINS DEPT OF CHEMISTRY F/G 20/8
OSF6 ENERGY LEVELS AND VIBRONIC COUPLING IN THE (DT2G)2 CONFIGU--ETC(U)
FEB 82 D L MICHALOPOULOS, E R BERNSTEIN N00014-79-C-0647
UNCLASSIFIED TR-6 NL

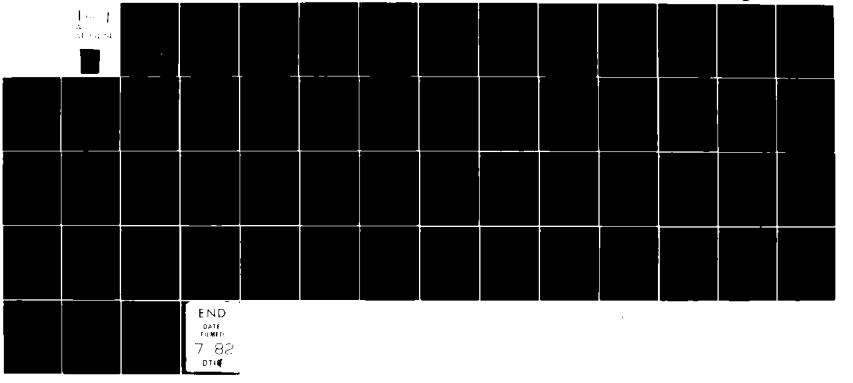

END
DATE FILMED
7 82
DTIC

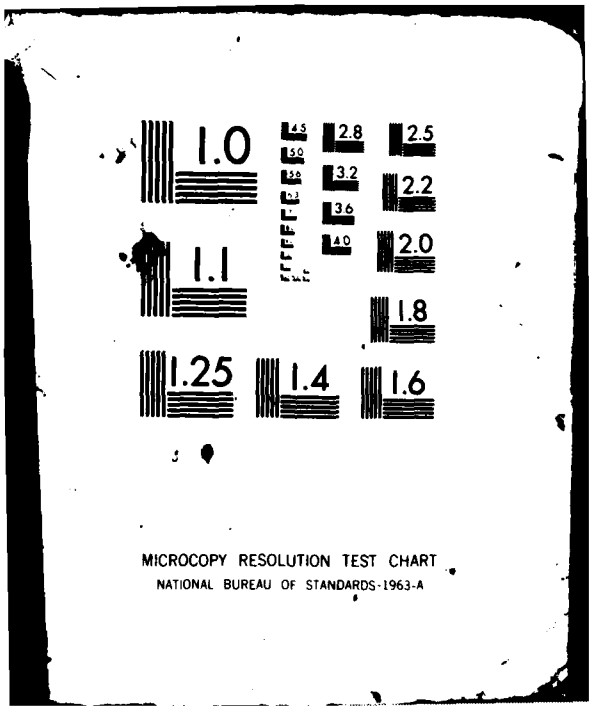
1.0
1.1
1.25
1.4
1.6
1.8
2.0
2.2
2.5
2.8
3.2
3.6
4.0
5.0
5.6
MICROCOPY RESOLUTION TEST CHART
NATIONAL BUREAU OF STANDARDS-1963-A

(12)

OFFICE OF NAVAL RESEARCH

Contract N00014-79-C-0647

Technical Report No. 6

OsF_6 ENERGY LEVELS AND VIBRONIC COUPLING in the $(d_{t_{2g}})^2$ CONFIGURATION

by

D.L. Michalopoulos and E.R. Bernstein

Prepared for Publication in

Molecular Physics

Department of Chemistry
Colorado State University
Fort Collins, Colorado 80523

2 February 1981

Unclassified

SECURITY CLASSIFICATION OF THIS PAGE (When Data Entered)

REPORT DOCUMENTATION PAGE	READ INSTRUCTIONS BEFORE COMPLETING FORM
1. REPORT NUMBER: Technical Report #6	2. GOVT ACCESSION NO.: AD-A115474
3. RECIPIENT'S CATALOG NUMBER	
4. TITLE (and Subtitle): OsF_6 Energy Levels and Vibronic Coupling in the $(d_{t_{2g}})^2$ Configuration	5. TYPE OF REPORT & PERIOD COVERED: Technical Report
	6. PERFORMING ORG. REPORT NUMBER
7. AUTHOR(s): D.L. Michalopoulos and E.R. Bernstein	8. CONTRACT OR GRANT NUMBER(s): N00014-79-C-0647
9. PERFORMING ORGANIZATION NAME AND ADDRESS: Department of Chemistry, Colorado State University, Fort Collins, Colorado 80523	10. PROGRAM ELEMENT, PROJECT, TASK AREA & WORK UNIT NUMBERS
11. CONTROLLING OFFICE NAME AND ADDRESS: Office of Naval Research, Arlington, VA 22217	12. REPORT DATE: May 26, 1982
	13. NUMBER OF PAGES: 51
14. MONITORING AGENCY NAME & ADDRESS (if different from Controlling Office)	15. SECURITY CLASS. (of this report)
	15a. DECLASSIFICATION DOWNGRADING SCHEDULE

16. DISTRIBUTION STATEMENT (of this Report)

Approved for Public Release; Distribution Unlimited

17. DISTRIBUTION STATEMENT (of the abstract entered in Block 20, if different from Report)

18. SUPPLEMENTARY NOTES

19. KEY WORDS (Continue on reverse side if necessary and identify by block number)

Jahn Teller Effect, Franck-Condon analysis, absorption spectra, Raman scattering, two-particle transitions, hexafluoride metals

20. ABSTRACT (Continue on reverse side if necessary and identify by block number)

Electronic and vibronic energy levels of the $(d_{2_{tg}})^2$ configuration of OsF_6 are studied using electronic Raman scattering and absorption spectroscopy. The ground state has been identified as E_g (crystal field split by ~28 cm^{-1}) and the first excited state is T_{1g} with crystal field energy levels at 14, 28 and 40 cm^{-1}. The three other regions of the spectrum that have been observed are at 4,000 cm^{-1}, 8,000 cm^{-1}, and 17,000 cm^{-1} covering the remaining $(d_{t_{2g}})^2$ configuration levels. The 4,000 cm^{-1} band consists of A_{1g} and T_{1g} electron states which do not interact strongly through vibronic coupling. The T_{1g} electronic state evidences a strong

DD FORM 1 JAN 73 1473 EDITION OF 1 NOV 65 IS OBSOLETE

20. ~(D 2.2) linear Jahn Teller effect for ν_5 and an observable Jahn Teller effect for ν_2. The band at 8,000 cm^{-1} consists of E_g and T_{2g} electronic states; it is so complex and strongly coupled that little information can be extracted from the absorption data concerning the Jahn-Teller interaction in this 5-fold degenerate manifold. The feature at 17,000 cm^{-1} is an A_{1g} electronic state and its elucidation follows normal behavior found in other hexafluoride spectra.

I. INTRODUCTION

Metal hexafluorides have been the objects of much study, both theoretical and experimental, in the last two decades. Two areas of particular interest have been the electronic spectra and structure of these molecules, and vibronic coupling. These interests have been sparked by the physical nature of the systems: low-lying electronic states with sharp assignable features, high molecular symmetry (O_h) resulting in electronic and vibrational degeneracies, and few vibrations (six) which obey known systematics.

Previous work with OsF_6 entailed a ground state vibrational analysis using absorption and Raman scattering data of gaseous and liquid samples.[1] These ground state frequencies are shown in Table I. The broad nature of $\nu_2(e_g)$ bands was interpreted as being the result of an $E_g \otimes e_g$ Jahn-Teller Effect (JTE).

Moffitt et al. obtained absorption spectra in the region between 4,000 and 50,000 cm^{-1} for gaseous OsF_6.[2] Three distinct types of band systems were observed. The first, found between 4,000 and 18,000 cm^{-1}, consists of three separate bands with irregular, well resolved vibrational patterns. Each of these three bands has an overall width on the order of 1,000 cm^{-1}. The second kind, between 35,000 and 40,000 cm^{-1}, with band widths of several thousand wavenumbers and little or no structure, are superimposed on a very intense continuum beginning at 22,500 and extending past 50,000 cm^{-1}. This continuum, the third band type, was assigned to states originating from the transfer of charge from the fluorine ligands to the central metal atom, while the first two were assigned as originating from the $(d_{t_{2g}})^2$ and $(d_{t_{2g}})^1(d_{e_g})^1$ electron configu-

rations, respectively. It is this first type of state, i.e., the $(d_{t_{2g}})^2$ ligand field states, which we report on in this paper.

As mentioned above, the hexafluorides possess electronic and vibrational degeneracy. They are expected, therefore, to evidence strong vibronic coupling. Recent work involving the Γ_8 electronic states of IrF_6[3,4,5,6] and ReF_6[7] have shown that standard linear Jahn-Teller (LJT) theory proves inadequate in describing the $\Gamma_8 \bullet e_g$ and $\Gamma_8 \bullet t_{2g}$ interactions. A coupling scheme including quadratic terms in the JT Hamiltonian and simultaneous treatment of both active vibrational modes was needed to explain spectral features.

A Franck-Condon analysis[8] of $\nu_5(t_{2g})$ progressions in the emission spectrum from the first charge transfer band of UF_6 (T_{ig} symmetry) has indicated a dominant $T_{ig} \bullet t_{2g}$ linear Jahn-Teller Effect (LJTE). We have found direct evidence from absorption data of a dominant $T_{1g} \bullet t_{2g}$ LJTE in the 4,000 cm^{-1} T_{1g} electronic state of OsF_6.

II. SUMMARY OF ELECTRONIC CALCULATIONS

In an effort to understand their experimental results, Moffitt and coworkers calculated the energies of the $(d_{t_{2g}})^2$ ligand field states of OsF_6.[2] Assuming little or no interaction between the $(d_{t_{2g}})^2$ and $(d_{t_{2g}})^1(d_{e_g})^1$ configurations, or between the $(d_{t_{2g}})^2$ configuration and charge transfer states, they were able to treat the problem as one involving an isolated manifold of $d_{t_{2g}}$ orbitals.

Moreover, due to the isomorphism between $(d_{t_{2g}})^n$ and atomic p^{6-n} configurations, the problem further reduced to spherical symmetry. The well known solution to this calculation involves two-parameters-spin orbit coupling and electron correlation. Indeed, it was found that the OsF_6 ligand field states are fit by a p^4 atomic configuration with spin orbit coupling and correlation being of the same magnitude-3,200 cm^{-1}.

Eisenstein[9], on the other hand, has done a calculation ignoring only the charge transfer states. Following the lines of a more conventional ligand-field calculation, he included a stereospecific potential due to the fluorine ligands, spin-orbit coupling, correlation, and configuration interaction. Subsequent diagonalization of the matrices obtained using the above interactions in an octahedral basis are compared in Table II to Moffitt's results. A schematic diagram of this method is shown in Figure 1. Two things should be noted: the group-theoretical correlation between the eigenstate representations in the spherical and octahedral bases and the predicted proximity of the members of the three pairs of states in the Eisenstein approach. Of course, these nearly degenerate states can only be distinguished from each other at low temperatures and high resolution.

III. SUMMARY OF PERTINENT JAHN-TELLER THEORY

The vibronic Hamiltonian for a $T_1 \bullet t_2$ LJTE is given by[10]

$$H(q,p) = \tfrac{1}{2}[P_\xi^2 + P_\eta^2 + P_\zeta^2 + W^2(q_\xi^2 + q_\eta^2 + q_\zeta^2 \,]\frac{L_\tau}{\sqrt{6}}\begin{pmatrix} 0 & q_\zeta & q_\eta \\ q_\zeta & 0 & q_\xi \\ q_\eta & q_\xi & 0 \end{pmatrix}.$$

Here, q and p are the coordinate and momentum vectors of the t_2 vibrational interaction. The term within the brackets is the Hamiltonian for an unperturbed three-dimensional harmonic oscillator.

Moffitt and Thorson, using second order perturbation theory, have obtained a solution for the vibronic level energies for small L_τ, i.e., $L_\tau << h\omega°$, in which $h\omega°$ is the energy of the unperturbed vibration. For $L_\tau \sim h\omega°$, perturbation methods fail, and a parametric calculation is required. Caner, Englman, and Toaff have done this calculation for a molecule of O symmetry in the following manner.[11]

Vibronic functions, spanning representations of the point group O, Γ_ν, with components γ_ν are given by:

$$|\Gamma_\nu,\gamma_\nu;\ \Gamma_\tau;\ n,\ell,s> = [\Gamma_\nu]^{\frac{1}{2}} \sum_{\rho,\gamma_\tau} V\begin{pmatrix} \Gamma_\tau & \Gamma_1 & \Gamma_\nu \\ \gamma_\tau & \rho & \gamma_\nu \end{pmatrix} |\Gamma_\tau,\ \gamma_\tau;\ n,\ell,s>|\rho>.$$

Here, Γ_τ and γ_τ are the representation and component of symmetry adapted vibrational functions; n and ℓ are the principal and angular

momentum vibrational quantum numbers; s is an index distinguishing different vibrational functions with same Γ_τ, γ_τ, n, and ℓ; the $V\begin{pmatrix}\Gamma_\tau & T_1 & \Gamma_\nu \\ \gamma_\tau & \rho & \gamma_\nu\end{pmatrix}$ are coupling coefficients for the point group O as defined by Griffith;[12] the $|\rho>$ are the three components of the T_1 electronic state; finally, $[\Gamma_\nu]$ is the degeneracy of the vibronic function. The symmetry adapted vibrational functions are linear combinations of spherical harmonics, Y_ℓ^m, defined and tabulated in the literature,[13] tranforming as representative of the point group O. The quantum numbers n and ℓ take on the values 0,1,2,... and n, n-2, n-4,...0 or 1 respectively.

A secular matrix is then constructed using these functions. Since the Hamiltonian is invariant under group operations, this matrix can be put immediately in block diagonal form. Each of these blocks contains functions spanning the same representation; there are five of these block matrices, of symmetry A_1, A_2, E, T_1 and T_2. Each matrix is then separately diagonalized; the vibronic eigenfunctions (of symmetries A_1, A_2, E, T_1 and T_2) and eigenvalues are thus generated. The eigenfunctions take the form

$$|\Psi_j^{\Gamma_\nu\ \gamma_\nu}> = \sum_{\Gamma_\tau,n,m,s} A(\Gamma_\nu,j;\ \Gamma_\tau;\ n,m,s)|\Gamma_\nu,\gamma_\nu;\Gamma_\tau;n,m,s>$$

in which j(=1,2,3...) labels different eigenfunctions with the same Γ_ν and γ_ν. The coefficients A are obtained directly from the calculation. The eigenvalues are shown, up to n=3, in Figure 2 as a

function of $L_T/\sqrt{6}\ h\omega°$. An alternate expression for coupling size is $D = \frac{1}{9}\frac{(L_\tau)^2}{(h\omega°)^2}$.

IV. EXPERIMENTAL

Experimental procedures are detailed elsewhere.[14,15] Briefly, appropriate molar quantities of host (MoF_6 or WF_6) and OsF_6 are distilled and mixed in a monel vacuum line (ultimate pressure : $1x10^{-7}$ torr), drawn into either a quartz or pyrex cell and glass blown off. The host materials are obtained commercially; OsF_6 is synthesized via direct combination of the elements at elevated temperature and pressure.[16] Single crystals are grown at temperatures (~-15°C) below the structural phase transition temperature of the host over a period of months, cooled slowly to 77°K and stored under liquid nitrogen until needed.

Absorption spectra, obtained at 1.8°K, 4.2°K, and 77°K, are taken with sample concentrations of .5% and 1% OsF_6. A one meter monochromator with appropriate grating and filtering is used. For infrared experiments, the apparatus included a Tungsten/Iodine lamp and liquid nitrogen cooled detector, while for visible absorption spectra a high pressure Xenon lamp and cooled photomultiplier tube are used.

Raman scattering spectra are obtained at 4.2°K and 77°K with sample concentrations ranging from 5% to 25% OsF_6. The light source is one of the lines of an Ar^+ laser; output powers at the

sample are set at 500 mW. Sample alignment is monitored by checking scattered light intensity from the host ground state ν_1 vibration; typical intensities are 100,000 cps for host ν, 1,000 cps for the 4,000 cm^{-1} A_{1g} OsF_6 electronic origin, 100 cps for the OsF_6 ν_1 vibration built on this origin. The scattered light is filtered by a 1/2 meter double monochromator with 1,800 gr/mm gratings and detected by a low dark count. high sensitivity photomultiplier tube. The monochromator is scanned by a Hewlett-Packard 9845A desktop computer, which also collects, averages, and stores data.

V. RESULTS AND DISCUSSION

A. Absorption Spectra

17,000 cm^{-1} A_{1g} State

A summary of experimental frequencies and assignments for the band are given in Table III. While the 77°K spectra are complicated by hot band structure, the 4.2°K trace of the A_{1g} electronic state in the visible, shown in Figure 3, is rather simple and exhibits many characteristics of metal hexafluoride systematics.

The sharp origin [Full-Width Half Height(FWHH) = 1 cm^{-1}], moderately intense due to the forced electric dipole nature of the transition, is surrounded by sharp, weak features [ΔE = + 5 to -5 cm^{-1}] which are assumed to be due to pair structure. While no concentration studies were attempted, this structure roughly mimics the

pair structure built on the A_{1g} origin at 4,000 cm^{-1}, on which concentration studies were carried out.

The most prominent features, the odd, Herzberg-Teller (HT) active vibrations, ν_6, ν_4, ν_3, are assigned because of their large intensities and through comparison with gas phase, ground state vibrational frequencies.

Two-particle transitions, similtaneous excitation of guest electronic state and host ground state vibration, appearing in this band as a broad shoulder to the blue of the ν_3 OsF_6 transition, involve both the ν_3 and ν_1 host vibrations. [See Table I for host vibrational frequencies]. High resolution, high dispersion spectra of this region yield the OsF_6 ν_1 transition, which is moderately weak and broad [FWHH ~ 3 cm^{-1}] presumably due to interaction with the host vibrations. The validity of this ν_1 assignment, agreeing with gas phase data, is enhanced by the appearance of the binary combinations $\nu_6 + \nu_1$, $\nu_4 + \nu_1$, and $\nu_3 + \nu_1$.

The fundamentals of the JT active vibrations, ν_2 and ν_5, are not observed as a result of parity selection rules. The fundamental frequencies, however, can be learned from odd-even binary combinations. Thus, from the $\nu_4 + \nu_5$ and $\nu_3 + \nu_5$ bands, it is seen that $h\omega_5^\circ$ = 220 cm^{-1}. Also, the weak feature at 766 cm^{-1} is assigned as a combination of host ν_6 and OsF_6 ν_2, yielding $h\omega_2^\circ$ = 626 cm^{-1}. These values for ν_2 and ν_5 can be used to gauge the strength of JT

interactions in the degenerate states, since it is expected that vibrational frequencies differ little between electronic ligand-field states.

Finally, no evidence of ν_1 progressions is seen, indicating similar geometries in ground and excited states. This is consistent with ReF_6 and IrF_6 data.[3-7]

4,000 cm^{-1} ($A_{1g} + T_{1g}$) Electronic Band

Spectra for this band were obtained for 1/2% and 1% OsF_6/MoF_6 and OsF_6/WF_6 samples at 77°K, 4.2°K and 1.8°K. Figure 4 shows a survey trace at 4.2°K. Table IV gives frequencies and assignments.

While there is little or no difference between 1.8 and 4.2°K spectra, two major differences are seen between 77°K and low temperature spectra. The high temperature spectra are broad, with origins of 3-5 cm^{-1} FWHH, presumably because the T_{1g} JT active potential surface is coupled to thermally populated host phonons; also, transitions are relatively weak with intensity distributed over several hot bands. On the other hand, the low temperature spectra show sharp features, with origins of 1 cm^{-1} FWHH, having somewhat more intensity and no hot band structure. Figure 5 compares origin regions at 77°K and 4.2°K.

Figure 6 compares the origin region for 1/2% OsF_6/WF_6 and 1% OsF_6/MoF_6 at 4.2°K. Of the four strong transitions present, the lowest in energy has pair structure built on it. Such an

assignment is evident of the non-linear relationship between OsF_6 concentration and the fine structure intensity. This would imply, based on selection rules, that this lowest transition is the A_{1g} origin, for one origin component of a degenerate electronic state is unlikely to carry pair structure while its partners do not. The remaining three features are assigned as being the components of the T_{1g} origin split by low symmetry crystal field of the solid. These assignments are supported by the Raman data presented in the next section. It should also be noted that the four transitions are shifted, relative to each other, in the different hosts as shown in Figure 6.

Assuming the lowest energy transition is the A_{1g} origin, it is straightforward to assign associated vibronic structure, as there is a strong resemblance to the visible A_{1g} band. No coupling between A_{1g} and T_{1g} states is apparent; this is not altogether unexpected for in the free molecule O_h configuration, inter-state vibronic coupling is group theoretically forbidden.

The low-temperature spectra of 1/2% OsF_6/WF_6 and 1% OsF_6/MoF_6 are nearly identical. Vibrations ν_6, ν_4, ν_3, and ν_1 are identified at 205, 275, 715, and 726 cm^{-1}, respectively. No evidence of ν_2 or ν_5 fundamentals is found; in the WF_6 spectra the binary combination $\nu_4 + \nu_5$ gives the ν_5 fundamental as 217 cm^{-1}. Combinations $\nu_6 + \nu_1$ and $\nu_4 + \nu_1$ are seen in both cases. Two-particle

transitions, involving host ν_4, ν_3, and ν_1 vibrations, obviously at different energies, are seen in both hosts. Vibrational site splittings are similar in both hosts: 1-5 cm^{-1} and 1.5-4 cm^{-1} in MoF_6 and WF_6 for ν_6 and ν_4, while no splitting on ν_3 is seen in either host. Finally, pair structure is carried on ν_4 and ν_6 in WF_6. The ν_6 pair structure in MoF_6 is most likely masked by the host broadened nature of the ν_6 transition. The fact that this pair structure is observed on the false origins is indicative of a ground state dimer interaction.[17]

The T_{1g} portion of the 4,000 cm^{-1} band is best analyzed by separating it into bending (ΔE = 0-500 cm^{-1}) and stretching (ΔE = 500-800 cm^{-1}) regions. The former is characterized by the crystal field split ν_6 false origin at 210 cm^{-1}. The expected intense ν_4 false origin is absent; however, very weak structure is present at ca. 275 cm^{-1}, and energetics suggest this is ν_4. More discussion of this point will follow. Figure 7 contains these features.

There is a great deal of host-independent structure in the region between 40 and 500 cm^{-1}. The host-independent nature of these features is verified by comparison of spectra taken in both hosts; moreover, these features are not explained by metal hexafluoride systematics as characterized in the A_{1g} electronic spectra. The most intense peaks, located at approximately 40, 120, 465 and 525 cm^{-1}, are shown in Figure 8. The first of these,

the most intense of the four, has a FWHH of 10 cm^{-1}; the possibility exists that this broad nature is due to the addition of host phonons on both the A_{1g} and T_{1g} origin components. It is seen in Figure 8 that this peak, though broad, is a singlet; the remaining three are obviously triplets, especially the one at 465 cm^{-1}.

Inspection of Englman's[11] calculation suggests that these features could result from a large, $T_1 \otimes t_2$ LJTE with $L_t/\sqrt{6}\ h\omega^\circ \tilde{=} 2.0$. Accordingly, the symmetry of these states would be A_2, T_2, T_1 and T_1, associated with vibrational principal quantum numbers, n, of 1,1,3, and 3. Other features in the bending region, though less intense, are seen to fit this concept of a LJTE. Indeed, we find that, though part of this region is partially obscured by the ν_6-ν_4 false origins, we are able to assign the majority (13) of the theoretical levels (up to n=3) to experimental data. A linear least squares fitting routine, used to maximize this fit, indicates $L/\sqrt{6}\ h\omega^\circ = 1.8$, D = 2.16. A value of 215 cm^{-1} was used for $h\omega_5^\circ$. The standard deviation of this fit is ~12 cm^{-1}. A comparison of calculated and experimental energies is shown in Table V.

It is interesting to note that the three intense degenerate states shown in Figure 8 are split on the order of 4-9 cm^{-1} by the solid; the origin and ν_6 vibration are split by roughly

25 and 15 cm^{-1}, respectively. This quenching of the low symmetry crystal field in JT states has been reported previously for the $\Gamma_8 \otimes (e_g + t_{2g})$ JTE in ReF_6.[7]

It should be stressed that the assignments leading to this fit were, for the most part, numerically obtained through energetics, and a LJTE, while evidentally dominant, is not necessarily the only mechanism present. As mentioned in Section I, quadratic terms become important for a $\Gamma_8 \otimes (e_g + t_{2g})$ JTE. For a Γ_8 electronic state, the LJT Hamiltonians have higher than molecular symmetry,[10] spherical for $\Gamma_8 \otimes t_{2g}$ and cylindrical for $\Gamma_8 \otimes e_g$; the quadratic Hamiltonians do not possess this pseudo-symmetry. Therefore, introduction of quadratic terms in the vibronic Hamiltonian for Γ_8 states leads to a reduction of the vibronic symmetries and a concomitant higher number of observed states. It is only necessary to count the number of vibronic transitions to detect the presence of a quadratic effect for Γ_8 states. However, for T_{ig} states, as in OsF_6 and UF_6, both linear and quadratic Hamiltonians possess octahedral symmetry only. There is no reduction in vibronic symmetry upon introduction of quadratic terms in the Hamiltonian and, consequently, no qualitative method to detect the influence of a quadratic effect. It is possible, therefore, that a quadratic effect may be present in the T_{1g} state. However, the data convincingly indicate a strong

linear effect; a quadratic effect can only be shown to contribute by a parametric calculation and, to date, the secular matrix needed for this calculation has not been constructed.

As mentioned in Section I, a dominant $T_{ig} \otimes t_{2g}$ LJTE has been shown to exist in UF_6 also, In this case the data, though not precluding a quadratic effect, only required a linear vibronic coupling Hamiltonian to be fit.

The low intensity of the ν_4 false origin for the T_{1g} can be understood in light of this JT interpretation. It is likely that there is a crystal-induced Fermi resonance between ν_4 and the nearby A_2 and T_2 Jahn-Teller components of ν_5. Although not seen in ReF_6, IrF_6, and the other OsF_6 states discussed in this paper, the mixing of ν_4 character into the ν_5 JT manifold probably is responsible for the large intensities of several of the ν_5 components. Another possible mechanism, a pseudo-JT effect seems unlikely; not only is it forbidden in zeroth order, but no perturbation of the 4,000 cm^{-1} A_{1g} band is observed in the spectra.

The stretching region of the T_{1g} band, shown in Figure 9, is rich in structure. Most of it is assignable to the A_{1g} electronic state as described earlier. The following are observed, however: ν_3 of the host in both MoF_6 and WF_6 and ν_1 of OsF_6 built on one of the T_{1g} origin components. Conspicuously absent are: the OsF_6 ν_3 false origin in either host or evidence of ν_2 either as a

fundamental or in a binary combination. The remaining structure in the stretching region is assigned, however, by default, to the ν_3/ν_2 manifold.

The nature of the data rules out any $T_{ig} \otimes e_g$ analysis. The absence of ν_3 may be due, in a fashion similar to the ν_5/ν_4 interaction, to an interaction between the components of ν_2 and ν_3.

Analysis of the hot band structure (see Fig. 5) leads to an assignment of the ground and first excited electronic states levels. There are three hot bands to the red of the A_{1g} origin. That these are built on this transition is verified by Raman data.

Since OsF_6 possess C_s site symmetry,[17] it is expected that the degeneracies of both the E_g and T_{2g} states would be fully removed. The presence of 3 instead of 4 hot bands indicates that an E_g and a T_{2g} component are accidentally degenerate. Accordingly, four models may be proposed, one with an E_g ground state, the others with a T_{2g} ground state. These are shown in Figure 10 along with their appropriate Boltzmann factors for 77°K.

Experimentally, the intensities of the A_{1g} origin transition and the second hot band are equal, while hot bands 1 and 3 are equal in intensity. The former are 10 times as intense as the latter. Assuming equal transition moments for transitions

originating from (low symmetry) components of the same state, model (b) predicts that hot band 1 should be 3/4 as intense as the origin transition, based on Boltzmann factors. This model is ruled out, therefore, as the actual intensity ratio is 0.1. Model(c)predicts that hot band 1 should have equal or greater intensity than the origin transition and therefore, can also be eliminated. Finally, model (d) predicts that hot bands 2 and 3 should be of similar intensities, thereby also eliminating it. The only model that cannot be conclusively ruled out by the data is (a). This model is even more attractive if the $A_{1g} \leftarrow E_g$ transition moment is assumed to be much larger than the $A_{1g} \leftarrow T_{2g}$ moment. The low lying electronic states are summarized as follows: the E_g state is assigned as the ground electronic state with a site splitting of 28 cm^{-1}; the T_{2g} state is the first excited electronic state; and the T_{2g} state is resolved into components at 14, 28, and 40 cm^{-1}. Such an assignment is further corroborated by the expected hot bands on the T_{1g} origin being superimposed on the existing A_{1g} origin and its hot bands as is shown in Figure 5.

8,000 cm^{-1} Band ($T_{2g} + E_g$)

This band violates the systematics seen in other low temperature absorption spectra of ReF_6, IrF_6, and OsF_6. A survey spectrum of the entire region is shown in Figure 11. The spectrum,

comprised of an envelope of transitions covering 800 cm^{-1}, can be qualitatively interpreted in the following manner. There is one origin with strong features at 120, 250, and 660 cm^{-1}. These are presumably the ν_6, ν_4, and ν_3 false origins. Note the discrepancies between these numbers and the frequencies measured in the two A_{1g} states and even the T_{1g} state. Other transitions, of the same magnitude of intensity as the false origins, at 320 and 460 cm^{-1}, are unassignable using known energetics. A weak feature at 719 cm^{-1} is assigned as ν_1. Finally, no possible interpretation of these transitions in terms of metal hexafluoride systematics results in reasonable locations for the missing origin components and more comprehensible values for false origin frequencies.

The absence of 4 of the 5 expected origin components is not due to selection rules. This judgment is based on two facts: no origin component of any degenerate electronic state is missing in any other low temperature spectra of IrF_6, ReF_6, or OsF_6, and the reduction of molecular symmetry by the solid (C_s site symmetry) tends to relax selection rules.

The quenching of electronic operators within ground or excited vibronic manifolds is well known.[18,19,20] One such operator is the low symmetry crystal field. Indeed, such an effect has been characterized in ReF_6 excited vibronic states.[7]

The complexity of the 8,000 cm^{-1} band structure indicates that both E_g and T_{2g} states are strongly involved in vibronic coupling. It is, therefore, interesting to examine the influence of a LJT effect on the crystal field splitting of the E_g and T_{2g} states.

The ground vibronic state Hamiltonians for these states are listed below.[18,20] Only low symmetry operators are included.

I. E • e LJTE

$$H = G(A_1)\,\underset{\approx}{I} + q\,G(E_\theta)\sigma_\vartheta$$

$$I = \begin{pmatrix} 1 & 0 \\ 0 & 1 \end{pmatrix} \quad \sigma_\theta = \begin{pmatrix} -1 & 0 \\ 0 & 1 \end{pmatrix}$$

II. T • e LJTE

$$H = G(A_1)\,\underset{\approx}{I} + G(E_\theta)\epsilon_\theta + K(T_2)[G(\xi)\,T_\xi + G(\eta)\,T_\eta + G(\zeta)\,T_\zeta]$$

$$\underset{\approx}{I} = \begin{pmatrix} 1 & 0 & 0 \\ 0 & 1 & 0 \\ 0 & 0 & 1 \end{pmatrix}; \quad \epsilon_\theta = \begin{pmatrix} \tfrac{1}{2} & 0 & 0 \\ 0 & \tfrac{1}{2} & 0 \\ 0 & 0 & -\tfrac{1}{2} \end{pmatrix}$$

$$T_\xi = -\begin{pmatrix} 0 & 0 & 0 \\ 0 & 0 & 1 \\ 0 & 1 & 0 \end{pmatrix}; \quad T_\eta = -\begin{pmatrix} 0 & 0 & 1 \\ 0 & 0 & 0 \\ 1 & 0 & 0 \end{pmatrix}; \quad T_\zeta = -\begin{pmatrix} 0 & 1 & 0 \\ 1 & 0 & 0 \\ 0 & 0 & 0 \end{pmatrix}$$

III. T • t_2 LJTE

$$H = G(A_1)\,\underset{\approx}{I} + K(E)G(E_\theta)\epsilon_\theta + K'(T_2)[G(\xi)T_\xi + G(\eta)\,T_\eta + G(\zeta)\,T_\zeta]$$

The operators represent the following solid state effects: $G(A_1)\ \underset{\approx}{I}$, gas to crystal shifts; $G(E_\theta)\sigma_\theta$ and $G(E_\theta)\varepsilon_\theta$, tetragonal ($D_{4h}$) distortion; $G(\xi)T_\xi$, $G(\eta)T_\eta$, and $G(\zeta)T_\zeta$, trigonal (D_{3d}) distortion. The G's are parameters expressing the size of the low symmetry crystal field. Finally, q, $K(T_2)$, $K(E)$ and $K'(T_2)$ are quenching factors which are dependent on the magnitude of the JTE.

These quenching factors have been calculated for LJT effects.[20]

1. $0.484 \leq q \leq 0.500$
2. $K(T_2) = \exp[^{-L^2}/(2\hbar\omega)^2] = \exp\ [^{-3E_{JT}}/(2\hbar\omega)]$
3. $K(E) \equiv \exp[^{-9E_{JT}}/(4\hbar\omega)]$
4. $K'(T_2) \equiv \frac{1}{3}(2 + \exp[^{-9E_{JT}}/(4\hbar\omega)]$

As can be seen, the tetragonal distortion related splitting of an E vibronic ground state is not elimiated by a E ⊗ e linear effect. However, in a T electronic state, for T ⊗ e linear effect, a trigonal distortion can be reduced to zero for a large interaction, while a tetragonal distortion is unaffected. Finally, for a T ⊗ t effect, a tetragonal distortion caused splitting is brought to zero for a large coupling, while the trigonal field related splitting is reduced to 2/3 of its value in the absence of a JTE. For example, for $E_{JT} = h\omega$, $K(E) = .11$ and $K'(T_2) = .78$; where $E_{JT} = 2h\omega$, $K(E) = .01$ and $K'(T_2) = .68$.

O'Brien[21] has also shown that $K(E) = K(T_2)$ for a T state coupled equally to both e_g and t modes and that $1.0 > K(E)$, $K(T_2) > 0.4$. Therefore, no T state origin splitting can be completely quenched in the case of equal $T \otimes e$ and $T \otimes t_2$ JT interactions.

Assuming that OsF_6 has either D_{4h} or C_s symmetry in the crystal,[17] the latter expressed as a sum of tetragonal and trigonal distortions, it is apparent that no linear effect can be responsible for a total quenching of origin crystal field splittings resulting in the observation of only one origin transition. We are thus unable to explain the absence of the other expected origin transitions.

B. Electronic Raman Spectra

Attempts were made to obtain Raman scattering spectra of the 8,000 cm^{-1}, 4,000 cm^{-1}, and first excited electronic states, along with the upper component of the E_g ground state. Of these, only spectra of the 4,000 cm^{-1} band were observed. A survey spectrum at 77°K is shown in Figure 12. Three features are present, an intense origin (1000 cps) along with weak structure at 250 cm^{-1} (30 cps) and at 700 cm^{-1} (100 cps). These are apparently the even vibrations ν_5, and/or ν_2, and ν_1.

At higher resolution, the origin is seen to consist of four transitions, as illustrated in Figure 13; at 4.2°K, only the transition highest in energy is observed. This latter feature

corresponds energetically to the A_{1g} origin in the absorption spectra and is so assigned. One vibrational peak is seen at 4.2°K; this feature, at 725 cm^{-1}, is obviously the totally symmetric vibration built on the A_{1g} origin. The value of $\hbar\omega$ = 725 cm^{-1} is quite close to the value of ν_1 observed in the absorption spectra. A summary of high and low temperature data is presented in Table VI.

The hot band structure associated with the origin corresponds to the hot band structure to the red of the A_{1g} origin in the 77°K absorption spectra. Accordingly, these features can be assigned to the transitions to the A_{1g} origin from the thermally populated upper component of the E_g ground state at 28 cm^{-1} and the 3 T_{2g} first excited state components at 14, 28, and 40 cm^{-1}. This gives an unperturbed approximate value of 30 cm^{-1} for the separation of ground and first excited states, consistent, at least qualitatively, with Eisenstein's calculation. Also, the two components at 28 cm^{-1} are accidentally degenerate in both MoF_6 and WF_6 hosts indicating the shift in them due to change in hosts is within the linewidth [FWHH ~ 7 cm^{-1}] of the Raman transition.

VI. CONCLUSIONS

Absorption and electronic Raman spectroscopy have been used to locate and study the electronic state of OsF_6. It is

found that previous electronic calculations are substantially correct. See Table I for comparison of low temperature data and calculational results. These data agree with Eisenstein's predictions of an E_g ground state and a T_{2g} first excited state nearly degenerate with it, and an $A_{1g} + T_{1g}$ band at roughly 4,000 cm^{-1} with the A_{1g} state being slightly lower in energy. Spectra of the 8,000 cm^{-1} band, however, do not explicitly show the presence of the predicted $T_{2g} + E_g$ origins and bands. The band observed violates MF_6 systematics, however, and it seems likely that it is heavily perturbed by vibronic coupling. The absence of expected origin transitions is not understood. Linear (or quadratic) Jahn-Teller effects alone do not seem responsible. Finally, we observe an A_{1g} electronic state at 16,900 cm^{-1} as predicted.

The two A_{1g} electronic state spectra are nearly identical in appearance and exhibit hexafluoride systematics. The A_{1g} states are characterized by:

1. one moderately intense origin with associated pair structure.
2. intense false origins, ν_6, ν_4, and ν_3.
3. a rather weak ν_1 transition.
4. ν_2, ν_5 not directly observed; identified, if at all, by binary combination energies.
5. low symmetry crystal field splittings of degenerate ν_6, ν_4.

and ν_3 are ~ 5 cm^{-1}.

6. vibrational energies essentially unchanged between states; gas-crystal vibrational shifts are small.
7. two particle transitions identified for ν_6, ν_4, and ν_3.
8. pair structure carried on the false origins indicating that dimer interactions are present in ground state.

It is found that the T_{1g} electronic state is involved in a dominant $T_{1g} \bullet t_{2g}$ LJTE with D ~ 2.2. A crystal induced Fermi resonance is observed between ν_4 and ν_5 JT components. This interaction apparently affects the intensity of several ν_5 components. Its affect on the ν_5 component energies is not known but appears to be small as indicated by the overall good fit between JT calculations and the experimental results. Finally, this dominant linear effect agrees with the dominant linear $T_{ig} \bullet t_{2g}$ effect reported for UF_6; on the other hand, quadratic effects have been reported for the Γ_8 states of ReF_6 and IrF_6.

REFERENCES

1. B. Weinstock, H.H. Claassen, and J.G. Malm, J. Chem. Phys. 32, 181 (1958).
2. W. Moffitt, G.L. Goodman, M. Fred, and B. Weinstock, Mol. Phys. 2, 109 (1959).
3. E.R. Bernstein and J.D. Webb, Mol. Phys. 37, 191 (1979).
4. E.R. Bernstein and J.D. Webb, Mol. Phys. 36, 1113 (1978).
5. E.R. Bernstein and J.D. Webb, Mol. Phys. 35, 1585 (1978).
6. E.R. Bernstein and J.D. Webb, Mol. Phys. 37 203 (1979).
7. Meredith, G.R., J.D. Webb, and E.R. Bernstein, Mol. Phys. 34, 995 (1977).
8. E.R. Bernstein, G.R. Meredith, and J.D. Webb, J. Chem. Phys. 68, 4066 (1978).
9. J.C. Eisenstein, J. Chem. Phys, 34, 310 (1961).
10. W. Moffitt and W. Thorson, Phys. Rev. 108, 1251 (1957).
11. R. Englman, M. Caner, and S. Toaff, J. Phys. Soc. Japan 29, 306 (1970).
12. J.S. Griffith, The Irreducible Tensor Method for Molecular Symmetry Groups (Prentice-Hall, London, 1962).
13. S.L. Altmann and A.P. Cracknell, Rev. Mod. Phys. 37, 19 (1965).
14. E.R. Bernstein and G.R. Meredith, J. Chem. Phys. 64, 375 (1976).
15. D.L. Michalopoulos, Ph.D. Thesis (Colorado State University, 1982).
16. B. Weinstock and J.C. Malm, J. Am. Chem. Soc. 80, 4466 (1958).
17. E.R. Bernstein and J.R. Meredith, J. Chem. Phys. 64, 395 (1976).
18. F.S. Ham, Electron Paramagnetic Resonance, ed. S. Geschwino (Plenum Press, New York, 1972), p.1.
19. M.D. Sturge, Solid State Physics, ed. F. Seitz, D. Turnbull, and H. Ehrenreich, (Academic Press, New York, 1967), Vol. 20, P. 91.
20. R. Englman, The Jahn Teller Effect in Molecules and Crystals, (Wiley-Interscience, London, 1972) pp. 19-124.
21. M.C.M. O'Brien, Phys. Rev. 187, 407 (1969).
22. E.R. Bernstein and G.R. Meredith, Chem. Phys. 24, 289 (1977).

TABLE I

Ground state vibrational energies for OsF_6, MoF_6, and WF_6. OsF_6 energies measured at room temperature with gas and liquid samples [Ref. 1]. MoF_6, WF_6 energies measured at 77°K with neat crystals [Ref. 22]; values shown here are averaged values of exciton energies. The stretching region includes ν_1, ν_2, and ν_3; the bending region includes ν_4, ν_5, and ν_6.

	$\nu_1(a_{1g})$	$\nu_2(e_g)$	$\nu_3(t_{1u})$	$\nu_4(t_{1u})$	$\nu_5(t_{2g})$	$\nu_6(t_{2u})$
OsF_6	733	632	720	268	252	200
MoF_6	742	645	718	265	320	140
WF_6	772	670	690	250	325	147

TABLE II

Comparison of calculated and experimental electronic energies. Moffitt's calculation employed a spherical basis and states are labeled by angular momentum quantum numbers J; Eisenstein's calculation employed the O_h symmetry of the molecule and states are labeled by O_h point group representation. Note the correlation between the J=2 state of Moffitt and the (E_g + T_{2g}) states of Eisenstein. Low temperature energies are corrected for approximate gas-to-crystal shifts to obtain free molecule energies. All energies are expressed as cm^{-1}.

STATES		CALCULATIONS		EXPERIMENTS	
O_h	R_3	Moffitt[a]	Eisenstein[b]	298°K[c]	4.2°K[d]
E_g	2	0	0	0	0
T_{2g}	2	0	122	<250	~100
T_{1g}	1	3,900	4,305	4,316	4,310
A_{1g}	0	4,270	4,327	4,371	4,370
T_{2g}	2		8,670	8,482	8,480
E_g	2	8,170	8,826	---	8,480
A_{1g}	0	16,300	17,383	17,301	17,300

a. ref. 10
b. ref. 9
c. ref. 10
d. ref. this work

TABLE III

Summary of absorption data for 16,900 cm^{-1} $A_{1g} \leftarrow E_g$ electronic transition at 4.2°K. Sample used was a 1% OsF_6/MoF_6 mixed crystal. Uncertainties are ± 0.2 cm^{-1}.

cm^{-1}(VAC)	FWHH[a]	I[b]	$\Delta E(0\text{-}0)(cm^{-1})$[c]	Assignments
16,912.55	1 cm^{-1}	W	-5.42	pairs + 0-0
16,915.54		W	-2.43	pairs + 0-0
16,917.97	1 cm^{-1}	S	0	0-0
16,918.84		M	0.87	pairs + 0-0
16,920.55		VW	2.58	pairs + 0-0
16,922.53	1 cm^{-1}	W	4.56	pairs + 0-0
17,115.23		W	197.26	pairs + ν_6
17,117.60	2.1 cm^{-1}	S	199.63	ν_6
17,119.16	2.1 cm^{-1}	S	201.19	ν_6
17,121.52		VW	203.55	pairs + ν_6
17,123.48		VW	205.51	pairs + ν_6
17,189.38		M	271.03	ν_4
17,193.93	3 cm^{-1}	S	275.96	ν_4
17,196.25		MS	278.28	ν_4
17,409.02		MW	491.02	$\nu_4 + \nu_5$; ν_5=215.06 cm^{-1}
17,611.54		S	693.57	ν_3
17,613.43		S	695.46	$\nu_3(h)$[d]
17,631.91		W	713.94	$\nu_3(h)$
17,646.67		M	728.70	ν_1
17,657.17		VW	739.20	$\nu_1(h)$
17,684.16		W	766.19	$\nu_6(h)+\nu_2$; ν_2=626.19 cm^{-1}

TABLE III (cont.)

cm^{-1}(VAC)	FWHH	I	$\Delta E(0\text{-}0)(cm^{-1})$	Assignments
17,834.77		MW	916.80	$\nu_3+\nu_5$; ν_5 = 223.23 cm^{-1}
17,849.35		MW	931.38	$\nu_6 + \nu_1$
17,911.31		MW	993.34	$\nu_4(h) + \nu_1(h)$
17,925.37		MW	1,007.40	$\nu_4 + \nu_1$
18,339.86		MW	1,421.89	$\nu_3 + \nu_1$

Footnotes

a. FWHH = Full Width Half Height

b. I = Intensity
   VW = Very Weak
   MW = Moderately Weak
   W = Weak
   M = Medium
   MS = Moderately Strong
   S = Strong
   VS = Very Strong

c. $\Delta E(0\text{-}0)$ energy differences measured relative to origin transition.

d. h = host

TABLE IV

Summary of absorption data for $(A_{1g} + T_{1g}) \leftarrow E_g$ electronic transition at 4,000 cm^{-1} at 4.2°K. Sample used was a 1% OsF_6/MoF_6. Uncertainties are ±0.1 cm^{-1}. See Table III for notation used. An A_{1g} or T_{1g} in the assignment column indicates the origin on which the transition is built. Vibronic symmetries are given in parentheses. All T_{1g} transition energies are measured from an average origin energy of 4,112.56 cm^{-1}.

cm^{-1}(VAC)	FWHH	I	$\Delta E(0\text{-}0)(cm^{-1})$	Assignments
4,078.13	.6	M	-8.34	A_{1g} + pairs
4,080.47		W	-6.00	A_{1g} + pairs
4,083.13		W	-3.34	A_{1g} + pairs
4,084.72		W	-1.75	A_{1g} + pairs
4,086.47	1.7	S	0	A_{1g} (0-0)
4,088.31	1.1	M	1.84	A_{1g} + pairs
4,089.40		M	2.93	A_{1g} + pairs
4,096.52	.9	W	10.05	A_{1g} + pairs
4,098.70	.5	M	0	T_{1g} origin
4,112.10	.6	S	0	T_{1g} origin
4,126.87	.9	S	0	T_{1g} origin
4,153.45	7.5	S	40.89	$T_{1g} + \nu_5(A_2)$
4,231.86		M	119.30	$T_{1g} + \nu_5(T_2)$
4,233.75		M	121.19	$T_{1g} + \nu_5(T_2)$
4,235.90		W	123.34	$T_{1g} + \nu_5(T_2)$
4,288.04		S	201.57	$A_{1g} + \nu_6$ + pairs
4,290.80	2.4	S	204.33	$A_{1g} + \nu_6$
4,291.91	6.0	S	205.44	$A_{1g} + \nu_6$

TABLE IV (cont.)

cm^{-1}(VAC)	FWHH	I	$\Delta E(0\text{-}0)(cm^{-1})$	Assignments
4,297.81	4.6	S	211.34	$A_{1g} + \nu_6$
4,300.96		M	214.49	$A_{1g} + \nu_6$ + pairs
4,314.13	3.3	S	201.57	$T_{1g} + \nu_6$
4,323.56	5.4	S	211.00	$T_{1g} + \nu_6$
4,327.86	4.8	S	215.30	$T_{1g} + \nu_6$
4,338.85		M	252.38	$A_{1g} + \nu_4(h)$
4,343.37		M	256.90	$A_{1g} + \nu_4(h)$
4,348.19		M	261.72	$A_{1g} + \nu_4(h)$
4,352.26		S	265.79	$A_{1g} + \nu_4(h)$
4,355.11		M	268.64	$A_{1g} + \nu_4(h)$
4,358.05		S	271.58	$A_{1g} + \nu_4(h)$
4,362.33		S	275.86	$A_{1g} + \nu_4$
4,363.95		S	277.48	$A_{1g} + \nu_4$
4,366.71		S	280.24	$A_{1g} + \nu_4$
4,368.52		M	282.05	$A_{1g} + \nu_4$
4,385.19		W	272.63	$T_{1g} + \nu_4$
4,387.17		VW	274.61	$T_{1g} + \nu_4$
4,391.45		MW	278.89	$T_{1g} + \nu_4$
4,409.57		W	297.01	$T_{1g} + 2\nu_5(A_2)$
4,435.29		MW	322.73	$T_{1g} + 2\nu_5(T_2)$
4,443.18	3.5	M	330.62	$T_{1g} + 2\nu_5(T_1)$
4,500.18		W	387.62	$T_{1g} + 2\nu_5(T_2)$
4,576.82		W	464.26	$T_{1g} + 2\nu_5(T_1)$
4,579.23		W	466.67	$T_{1g} + 2\nu_5(T_1)$
4,583.11		W	470.55	$T_{1g} + 2\nu_5(T_1)$

TABLE IV (cont.)

cm^{-1}(VAC)	FWHH	I	$\Delta E(0\text{-}0)(cm^{-1})$	Assignments
4,589.95		M	477.39	$T_{1g} + 3\nu_5(T_1)$
4,592.69	2.2	M	480.13	$T_{1g} + 3\nu_5(T_1)$
4,594.28		M	481.72	$T_{1g} + 3\nu_5(T_1)$
4,597.02		W	484.46	$T_{1g} + 3\nu_5(A_2)$
4,602.95		W	490.39	$T_{1g} + 3\nu_5(A_1)$
4,616.66		W	504.10	$T_{1g} + 3\nu_5(E)$
4,620.40		W	507.84	$T_{1g} + 3\nu_5(E)$
4,636.25	16.0	M	523.69	$T_{1g} + 3\nu_5(T_1)$
4,640.02	16.0	M	527.92	$T_{1g} + 3\nu_5(T_1)$
4,645.73	16.0	M	533.17	$T_{1g} + 3\nu_5(T_1)$
4,689.31		W	576.75	$T_{1g} + 3\nu_5(A_2)$
4,783.90	9.0	M	697.43	$A_{1g} + \nu_3(h)$
4,786.30	9.0	M	699.83	$A_{1g} + \nu_3(h)$
4,801.82	4.3	S	715.35	$A_{1g} + \nu_3$
4,804.82		W	718.35	$A_{1g} + \nu_3(h)$
4,812.34	1.0	M	725.87	$A_{1g} + \nu_1$
4,813.84		W	701.28	$T_{1g} + \nu_3(h)$
4,816.74		W	704.18	$T_{1g} + \nu_3(h)$
4,820.34		M	707.78	$T_{1g} + \nu_3(h)$
4,827.56	1.0	S	741.09	$A_{1g} + \nu_1(h)$
4,833.75		W	721.19	$T_{1g} + \nu_3/\nu_2$
4,836.90		W	724.34	$T_{1g} + \nu_3/\nu_2$
4,847.22		W	760.75	$A_{1g} + \nu_3(h)$ + phonon(66 cm^{-1})
4,850.63	5.0	MS	764.16	$A_{1g} + \nu_3(h)$ + phonon(66 cm^{-1})
4,853.22		M	766.75	$A_{1g} + \nu_3(h)$ + phonon(66 cm^{-1})

TABLE IV (cont.)

cm^{-1}(VAC)	FWHH	I	$\Delta E(0\text{-}0)(cm^{-1})$	Assignments
4,863.85	10.0	MS	777.37	$A_{1g} + \nu_3(h)$ + phonon(83 cm^{-1})
4,867.40		M	780.93	$A_{1g} + \nu_3(h)$ + phonon(83 cm^{-1})
4,876.42		W	763.86	$T_{1g} + \nu_3/\nu_2$
4,883.09		W	770.53	$T_{1g} + \nu_3/\nu_2$
4,894.21		M	781.65	$T_{1g} + \nu_3/\nu_2$
4,934.92		W	822.36	$T_{1g} + \nu_3/\nu_2$
5,007.21	4.5	VS	920.74	$A_{1g} + \nu_6 + \nu_1$
5,015.63	3.0	M	903.07	$T_{1g} + \nu_3/\nu_2$
5,017.77		M	905.21	$T_{1g} + \nu_3/\nu_2$
5,038.13		M	925.57	$T_{1g} + \nu_3/\nu_2$
5,041.18		M	928.62	$T_{1g} + \nu_3/\nu_2$
5,047.67		W	935.11	$T_{1g} + \nu_3/\nu_2$
5,051.62		M	939.06	$T_{1g} + \nu_3/\nu_2$
5,055.45	8.8	S	942.89	$T_{1g} + \nu_3/\nu_2$
5,057.37		M	944.81	$T_{1g} + \nu_3/\nu_2$
5,077.92	11.3	S	991.45	$A_{1g} + \nu_4 + \nu_1$
5,079.08	11.3	S	992.61	$A_{1g} + \nu_4 + \nu_1$
5,081.66	11.3	S	995.19	$A_{1g} + \nu_4 + \nu_1$
5,085.54	11.3	M	999.07	$A_{1g} + \nu_4 + \nu_1$
5,089.04	11.3	M	1,002.57	$A_{1g} + \nu_4 + \nu_1$

TABLE V

Comparison of Englman, Caner, and Toaff's $T_1 \otimes t_2$ LJT calculation for a molecule of O-symmetry and OsF_6 transitions in the 4,000 cm^{-1} band. A linear fitting routine was used to obtain a D of ~ 2.0. Spectra were taken at 4.2°K with a 1% OsF_6/MoF_6 sample.

cm^{-1}(VAC)	$\Delta E(0\text{-}0)^{\dagger}$	ΔE(AVE)	Calc.	Vibronic Symmetry	$n^{\ddagger}$
4,153.45	40.89		41.35	$A_2^{\ddagger}$	1
4,231.86	119.30				
4,233.75	121.19	121.28	132.30	$T_2^{\ddagger}$	1
4,235.90	123.34				
4,409.57	297.01		305.95	A_2	2
4,435.29	322.73		318.36	T_2	2
4,442.18	330.62		334.89	T_1	2
4,500.18	387.62		384.51	T_2	2
4,576.82	464.26	467.16	434.12	T_1	2
4,583.11	470.55				
4,589.95	477.39				
4,592.69	480.13	479.75	442.39	$T_1^{\mp}$	3
4,594.28	481.72				
4,597.02	484.46		454.80	A_2	3
4,602.95	490.39		463.06	A_1	3
4,616.66	504.10	505.97	487.87	E	3
4,620.40	507.84				
4,636.25	523.69				
4,640.02	527.92	528.26	512.68	$T_1^{\ddagger}$	3
4,645.73	533.17				
4,689.31	576.75		587.10	A_2	3

TABLE V (cont.)

Footnotes

† measured from averaged origin energy of 4,112.56 cm^{-1}

‡ transitions shown in figure

‡ principal vibrational quantum number

TABLE VI

Comparison of $A_{1g} \leftarrow E_g$ Raman scattering data for 77°K and 4.2°K. Sample is a 5% OsF_6/MoF_6 mixed crystal. Slidwidths are on the order of 5 cm^{-1} for 77°K and 10 cm^{-1} for 4.2°K spectra due to low intensities of transitions. Energies are certain to ± 0.2 cm^{-1}. The origin and 3 hot bands of the 77°K spectra agree with infrared absorption data, as do the origin and ν_1 transition in the 4.2°K spectra.

Stokes Shift (VAC cm^{-1})	FWHH	I	ΔE(0-0)	Assignments
		77°K		
4,044.11		M	-44.90	hb, T_{2g} 1st excited state
4,060.68	7 cm^{-1}	S	-28.33	hb, T_{2g} 1st excited state, E_g ground state component
4,074.84		W	-14.17	hb, T_{2g} 1st excited state
4,089.01	7 cm^{-1}	S	0	A_{1g} 0-0
4,297.02		W	208.01	ν_5 + hb
4,328.49		W	239.48	ν_5 + hb
4,353.54		W	264.53	ν_5 + hb
4,386.45		W	297.44	ν_5 + hb
4,418.11		W	329.10	ν_5 + hb
4,764.05		W	675.04	ν_1 + hb (T_{2g} 1st excited state)
4,794.14		W	705.13	ν_1 + hb (T_{2g} 1st excited state)
4,804.85	5 cm^{-1}	MW	715.84	ν_1
		4.2°K		
4,082.77		W	-7.06	pairs
4,089.83	8.5 cm^{-1}	S	0	A_{1g} 0-0
4,103.01		W	13.18	pairs
4,807.74	8.5 cm^{-1}	MW	724.97	ν_1

FIGURE CAPTIONS

Figure 1

A schematic diagram showing the effect of an octahedral ligand field, spin orbit coupling, and electron correlation on a $(d_{t_{2g}})^2$ electronic configuration. Note the predicted near degeneracies of the pairs of states at 0, 4,000, and 8,000 cm^{-1}.

Figure 2

Jahn-Teller energies as a function of coupling parameter L_τ for a $T_2 \otimes t_2$ LJTE for a molecule of O-symmetry. Subscripts 1 and 2 should be interchanged for a $T_1 \times t_2$ effect, e.g., the 4,000 cm^{-1} T_{1g} state of OsF_6. [Reproduced with permission, R. Englman, "The Jahn-Teller Effect in Molecules and Crystals", (Wiley Interscience, London, 1972) p. 72.]

Figure 3

Survey absorption spectrum for the 16,900 cm^{-1} $A_{1g} \leftarrow E_g$ transition of OsF_6 at 4.2°K using a 1% OsF_6/MoF_6 sample. This spectrum exhibits many of the features characterizing hexafluoride systematics.

Figure 4

Survey absorption spectrum of the 4,000 cm^{-1} $(A_{1g} + T_{1g}) \leftarrow E_g$ transition of OsF_6 at 4.2°K using a 1% OsF_6/MoF_6 sample. Note the complexity of the band as compared to the 16,900 cm^{-1} A_{1g} band due primarily to the presence of the T_{1g} state.

Figure 5

A comparison of the 4,000 cm^{-1} $(A_{1g} + T_{2g})$ origin at 77°K and 4.2°K for a 1% OsF_6/MoF_6 sample. Note the hot bands to the red of the A_{1g} origin. See text for the hot band analysis leading to ground and first excited electronic state assignments. The stick diagram shows that hot bands built on the T_{1g} origin components are superimposible on the other transitions in the figure. The weak features built on the A_{1g} origin are assigned as pair structure.

Figure 6

A comparison of 4,000 cm^{-1} ($A_{1g} + T_{1g}$) origin at 4.2°K for .5% OsF_6/WF_6 and 1% OsF_6/MoF_6 samples. The nonlinear relationship between OsF_6 concentration and the fine structure intensity about the A_{1g} origin indicates the structure is due to pairs, etc.

Figure 7

The bending/false origin region of the 4,000 cm^{-1} ($A_{1g} + T_{1g}$) ← E_g at 4.2°K for a 1% OsF_6/MoF_6 sample. Note the weak intensity of the ν_4 false origin built on the T_{1g} electronic origin. See text for explanation. The $T_{1g} + \nu_4$ transition is broadened by interaction with the host ν_4.

Figure 8

Four moderately intense features of ($A_{1g} + T_{1g}$) ← E_g transition shown at 4.2°K for a 1% OsF_6/MoF_6 sample. These are assigned as components of ν_5 which is perturbed by a $T_{1g} \times t_2$ LJTE with D ~ 2.2. See text for discussion.

Figure 9

The stretching region of the 4,000 cm^{-1} ($A_{1g} + T_{1g}$) ← E_g transition at 4.2°K for a 1% OsF_6/MoF_6 sample. Note that most of the transitions assignable are features built on the A_{1g} origin. Assignments of ν_2/ν_3 built on the T_{1g} origin are made by default.

Figure 10

Four proposed models explaining hot band structure of 4,000 cm^{-1} A_{1g} ← ($E_g + T_{2g}$) absorption transition. The arrows represent absorption transitions from the ground ($E_g + T_{2g}$) states to the A_{1g} origin. Both the E_g and T_{2g} states are assumed split by the low symmetry crystal field. Boltzman factors (relative populations) are given for each level at 77°K. Model (a) is the only model not ruled out by intensity patterns.

Figure 11

A survey absorption spectrum of the 8,000 cm^{-1} ($E_g + T_{2g}$) ← E_g transition. This system evidences none of the usual hexafluoride vibronic patterns, presumably due to vibronic coupling. The origin transition, false origins, and ν_1 are indicated.

Figure 12

A survey Raman spectrum of 4,000 cm^{-1} ($A_{1g} + T_{1g}$) at 77°K for a 5% OsF_6/MoF_6 sample. Intensities are 1000 cps for the origin, 30 cps for ν_5, and 100 cps for ν_1.

Figure 13

High resolution spectrum of 4,000 cm^{-1} ($A_{1g} + T_{1g}$) origin region at 77°K for a 5% OsF_6/MoF_6 sample. The highest energy feature is the A_{1g} origin. The other three features are hot bands.

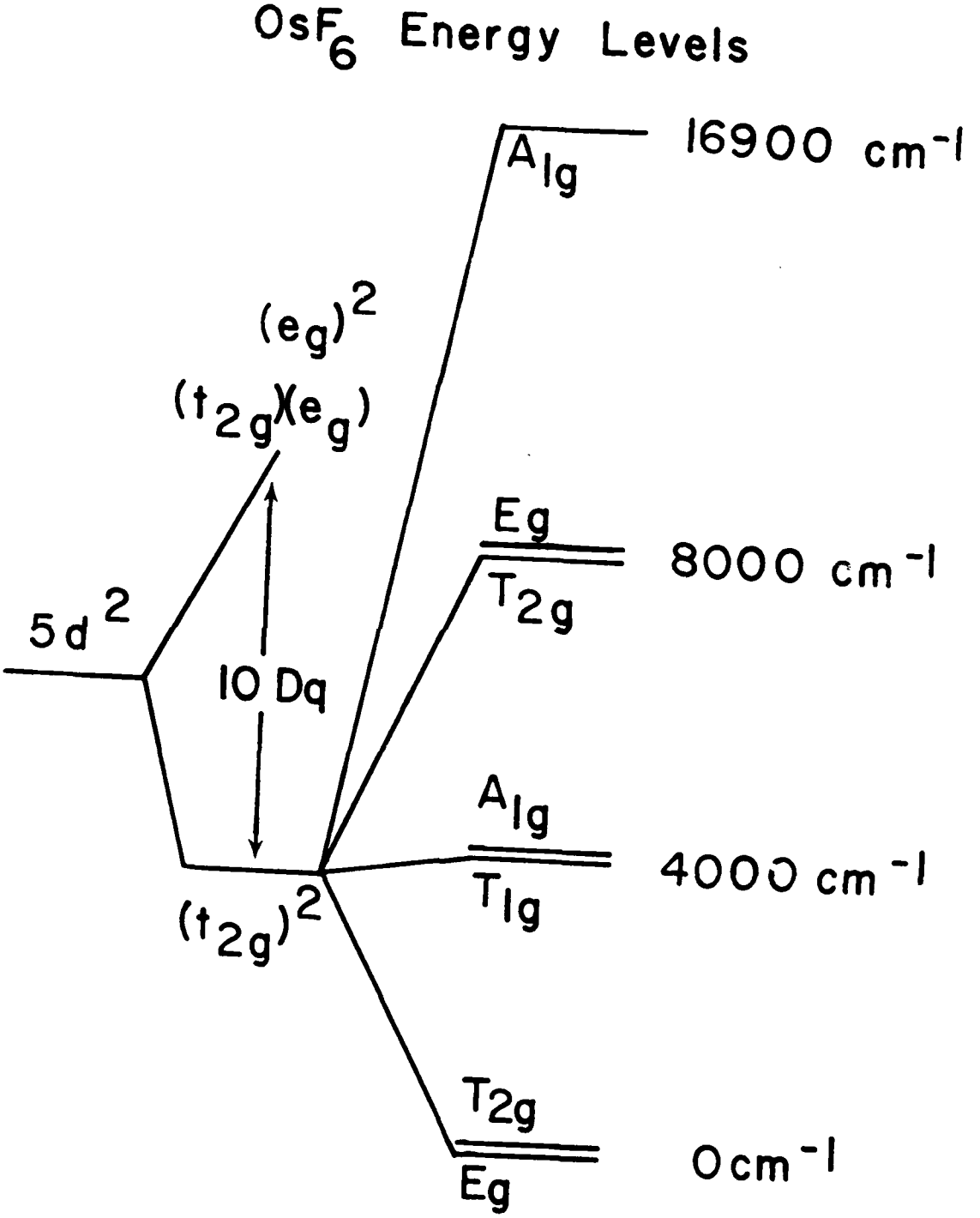
OsF6 Energy Levels
16900 cm-1
A1g
(eg)2
(t2g)(eg)
Eg
T2g
8000 cm-1
5d2
10 Dq
A1g
T1g
4000 cm-1
(t2g)2
T2g
Eg
0cm-1

$H_O + H_{cf} + (H_{so} + H_c)$

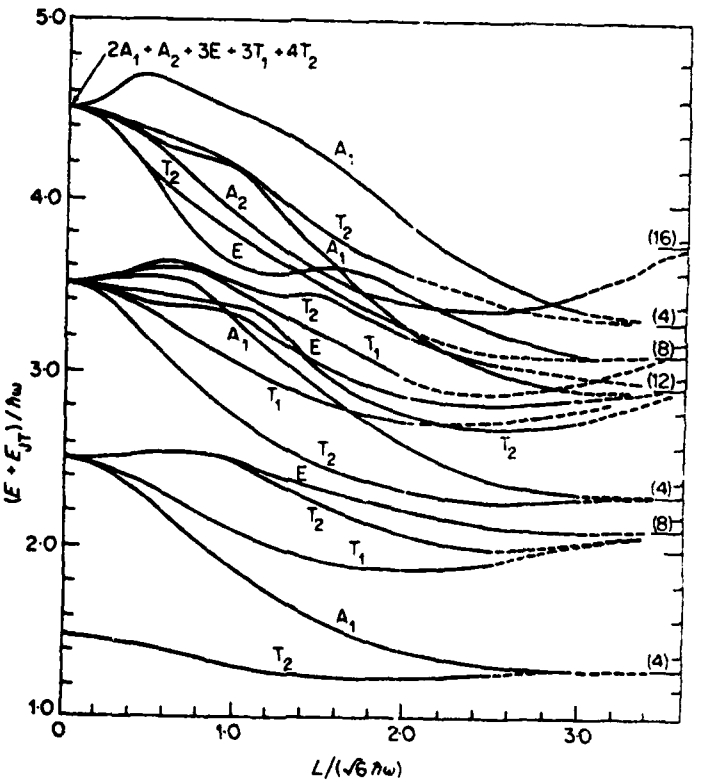
5·0
4·0
3·0
2·0
1·0
0
1·0
2·0
3·0
$2A_1 + A_2 + 3E + 3T_1 + 4T_2$
A_1
T_2
A_2
E
T_1
(16)
(4)
(8)
(12)
$(E + E_{JT})/\hbar\omega$
$L/(\sqrt{6}\hbar\omega)$

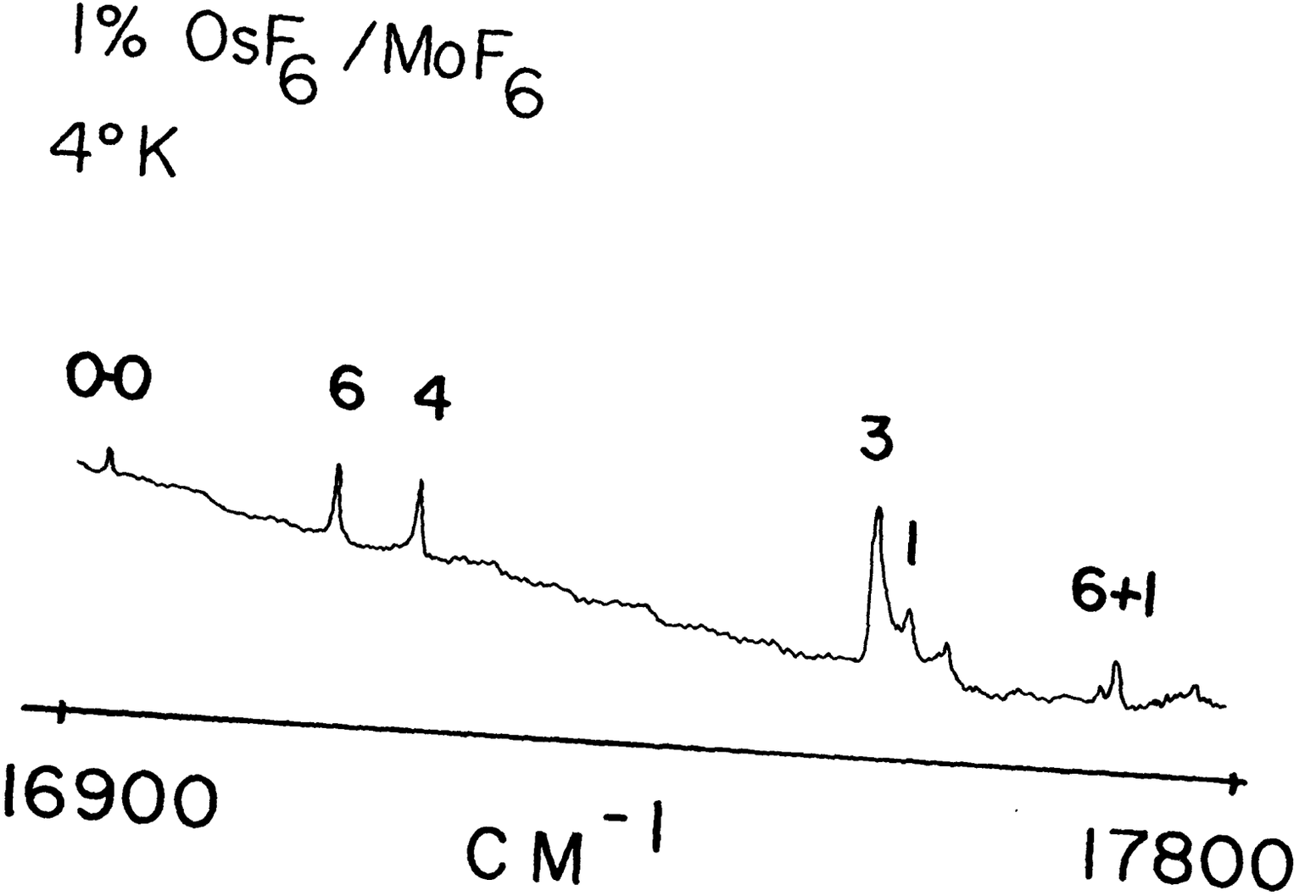
1% OsF_6 / MoF_6
4°K
00
6
4
3
1
6+1
16900
CM^{-1}
17800

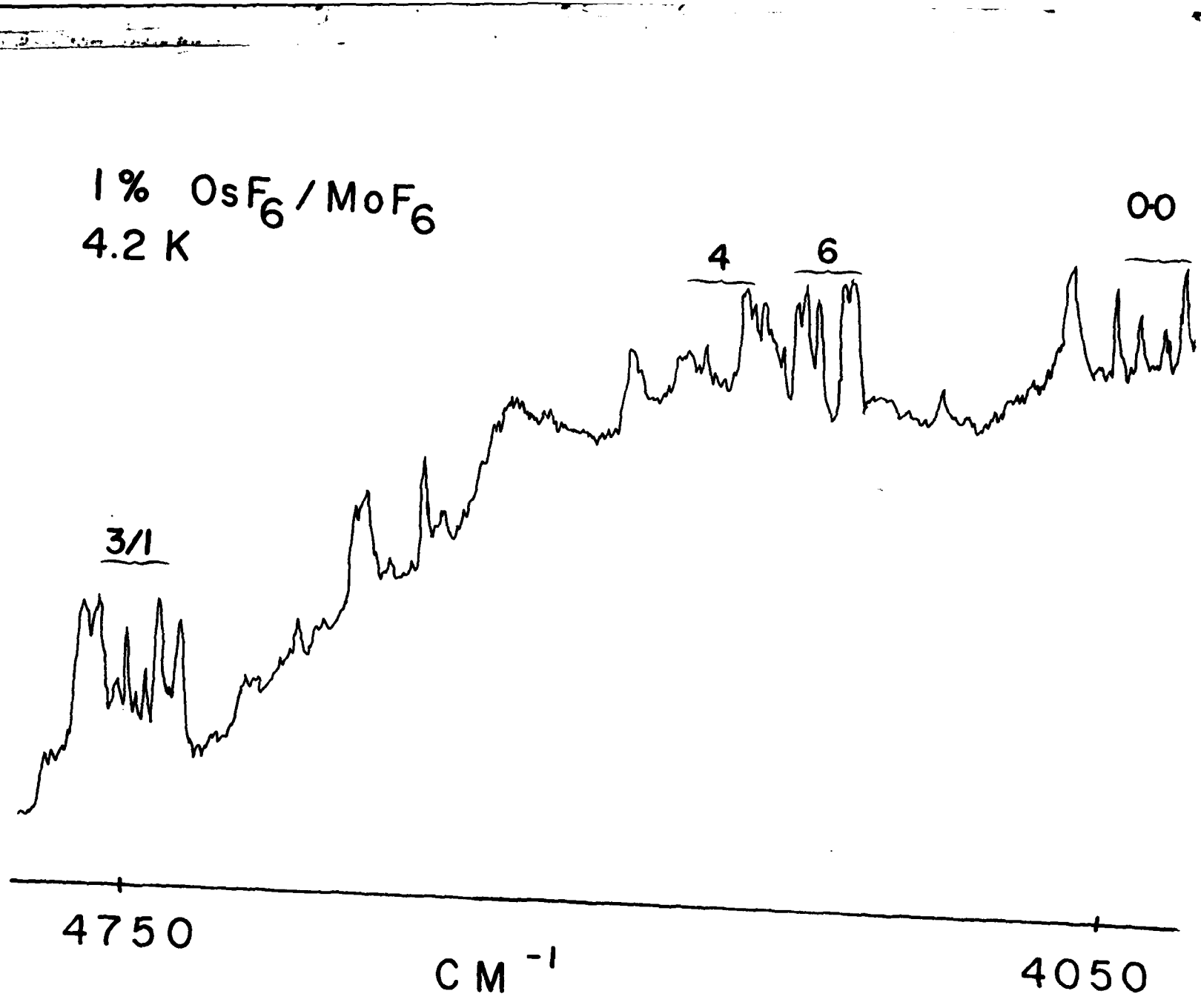
1% OsF_6 / MoF_6
4.2 K
0-0
4
6
3/1
4750
CM^{-1}
4050

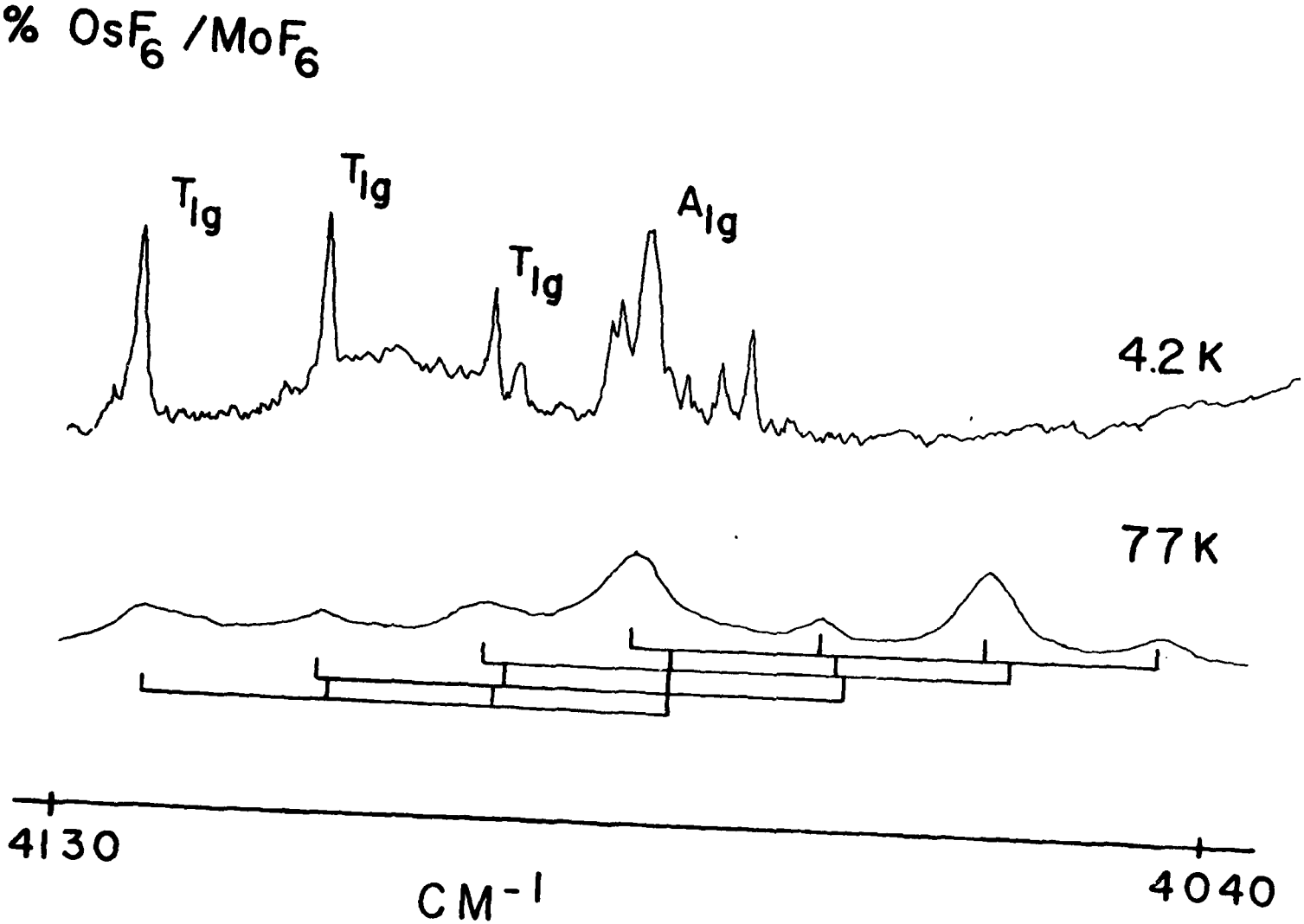
1% OsF_6 /MoF_6
T_{1g}
T_{1g}
T_{1g}
A_{1g}
4.2 K
77 K
4130
CM-1
4040

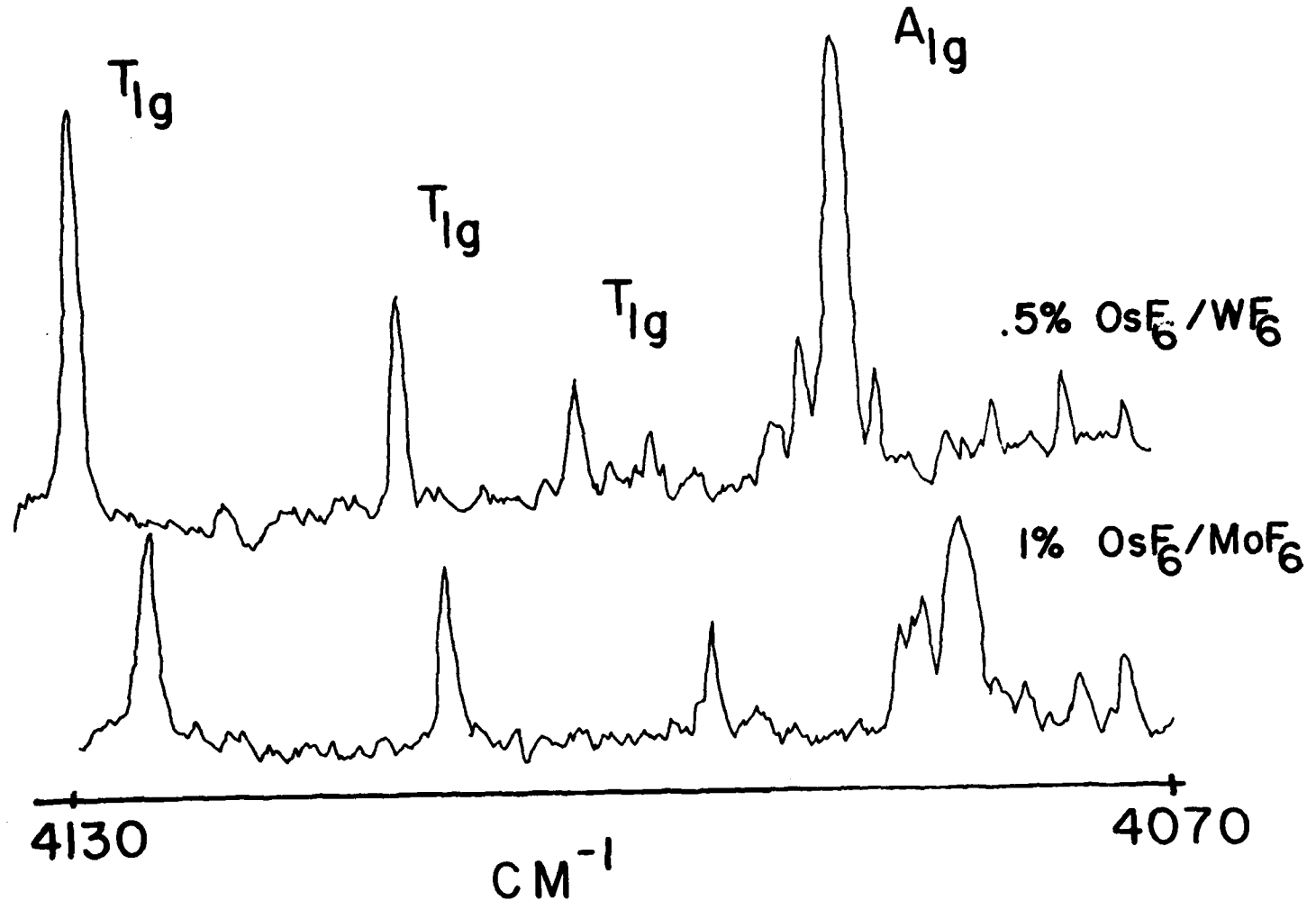
4.2 K
T_{1g}
T_{1g}
T_{1g}
A_{1g}
.5% OsF_6/WF_6
1% OsF_6/MoF_6
4130
4070
CM^{-1}

1% OsF_6/MoF_6

4.2 K

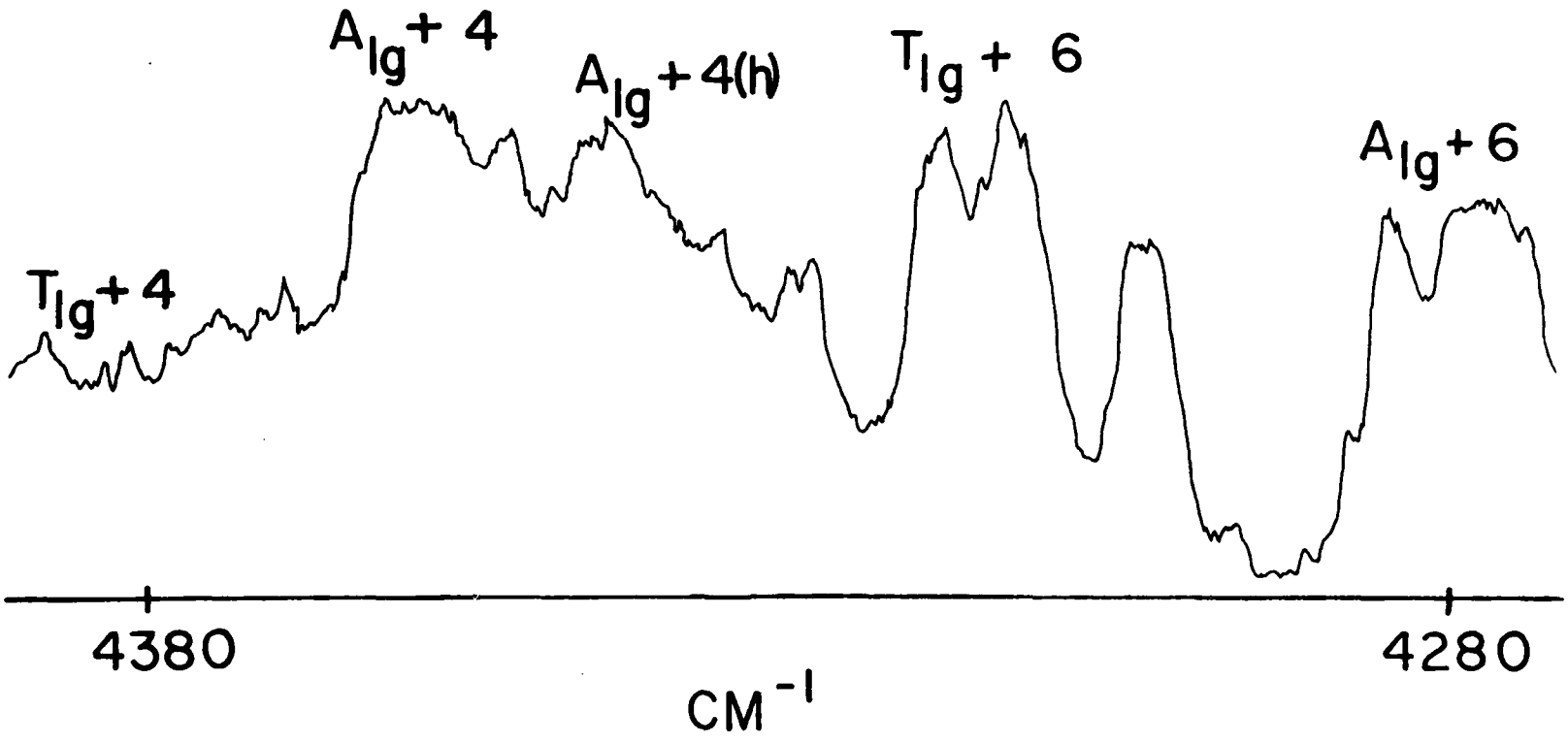

1% OsF_6 / MoF_6

4.2°K

$T_{1g} + \nu_5$

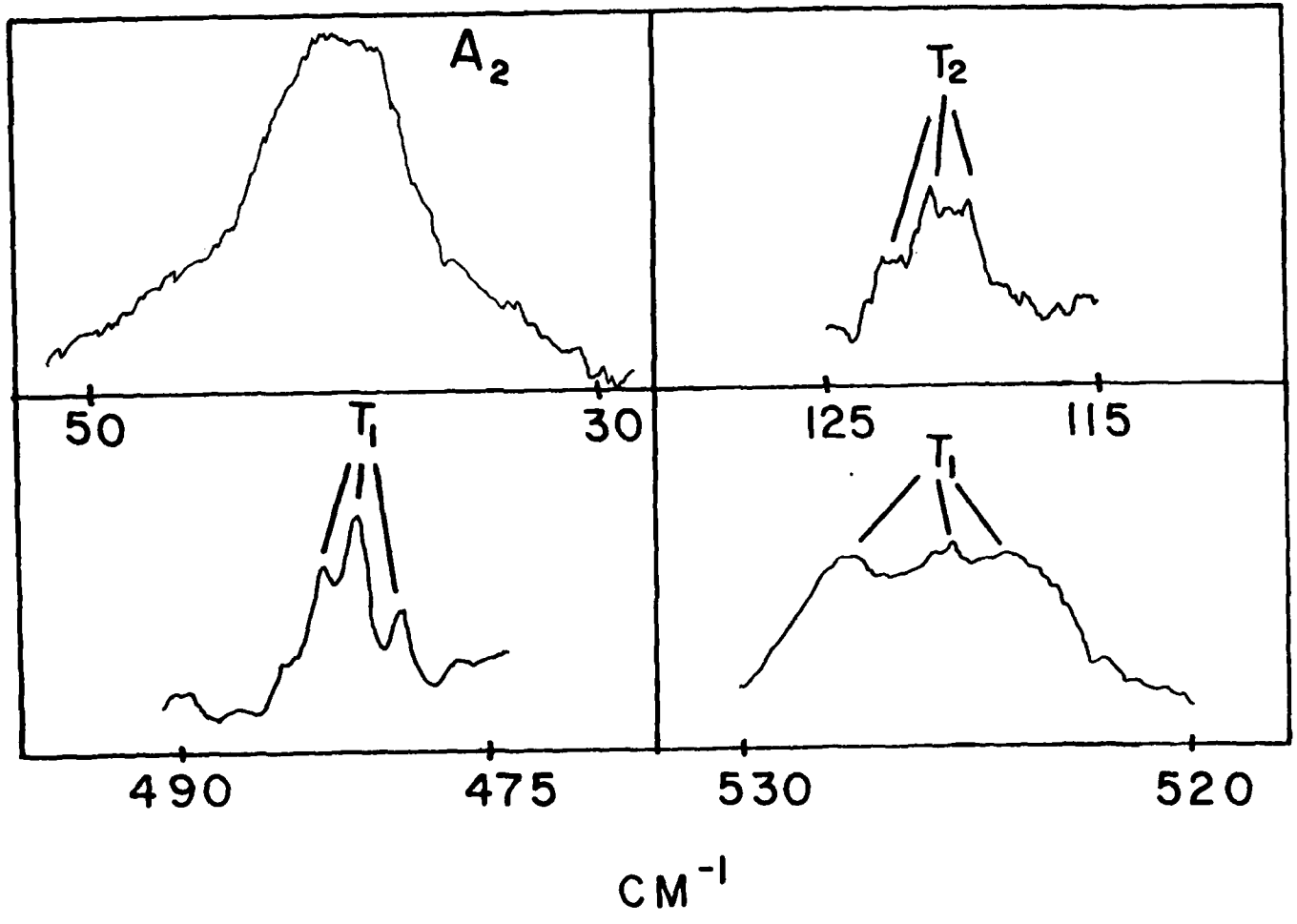

1% OsF_6/MoF_6

4.2 K

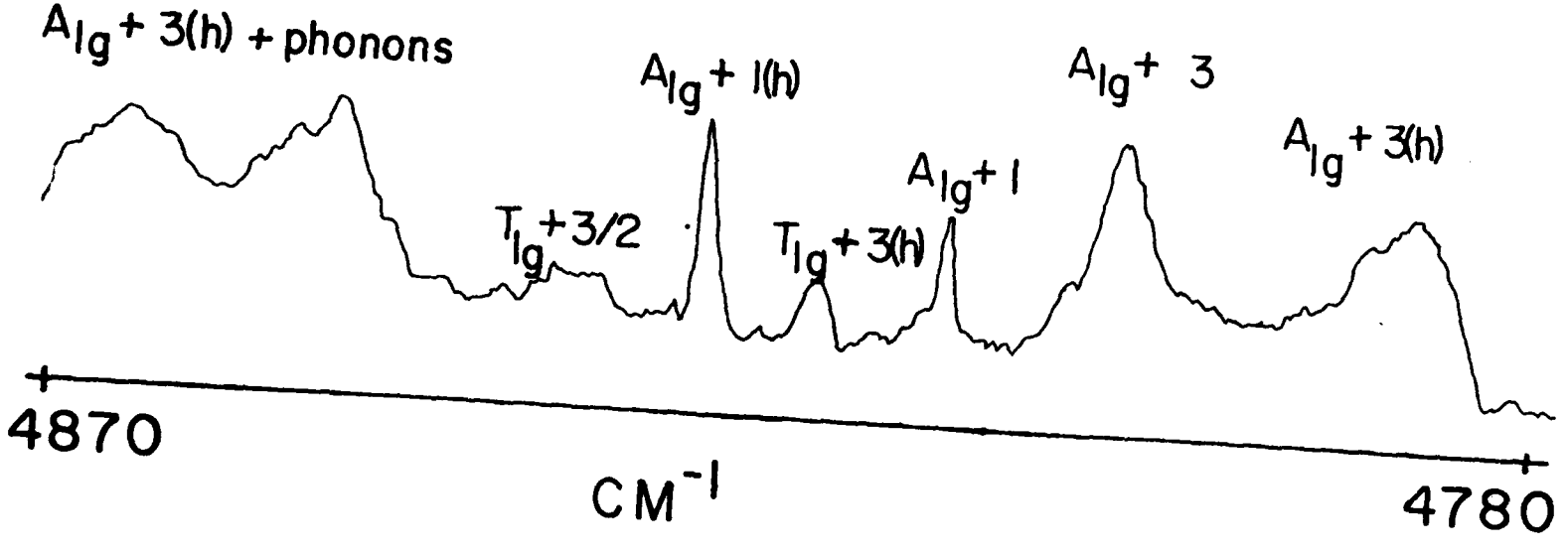

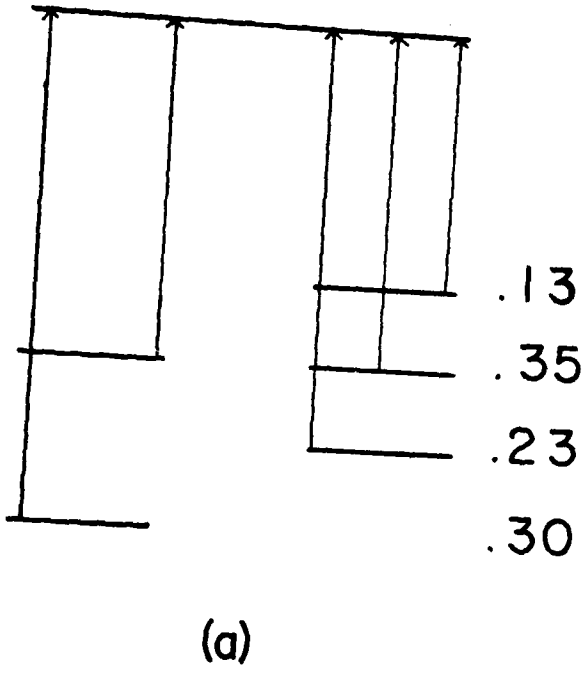

(a)

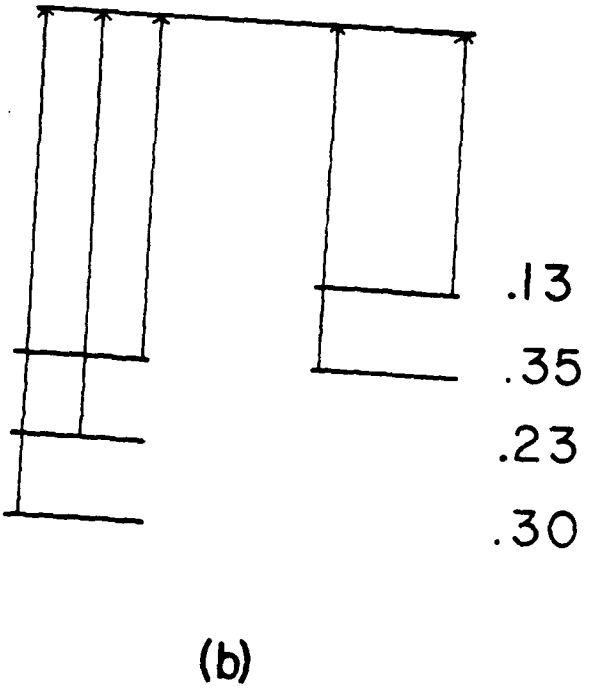

(b)

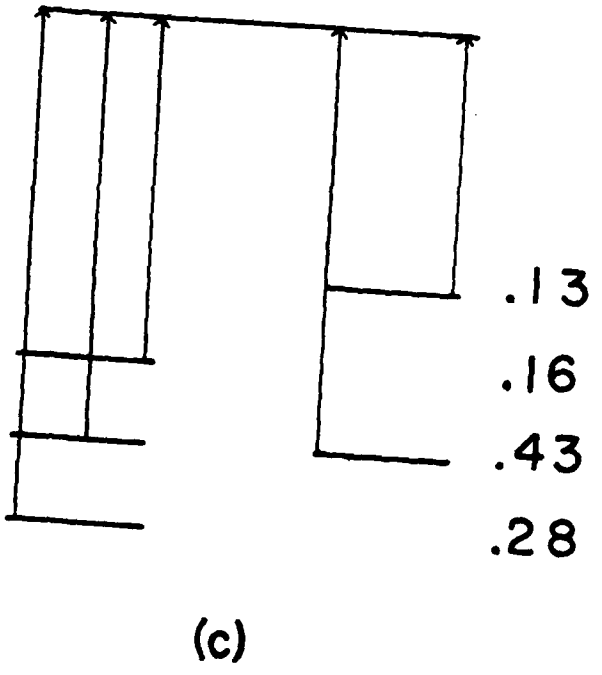

(c)

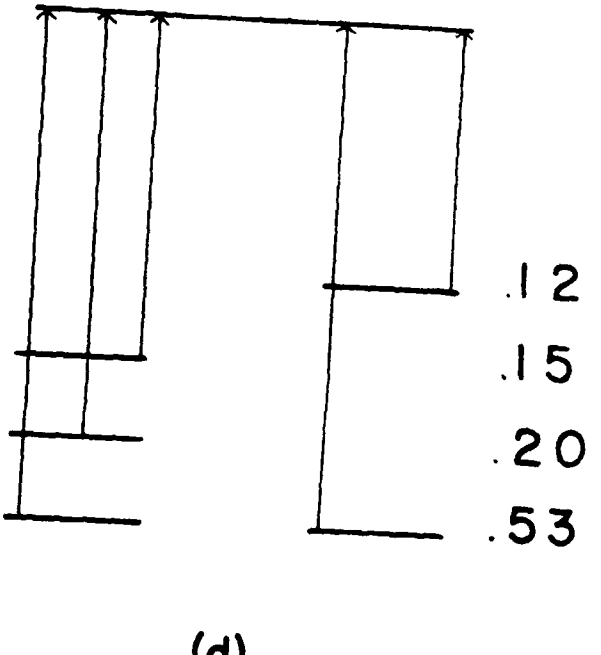

(d)

1% OsF_6/MoF_6

4°K

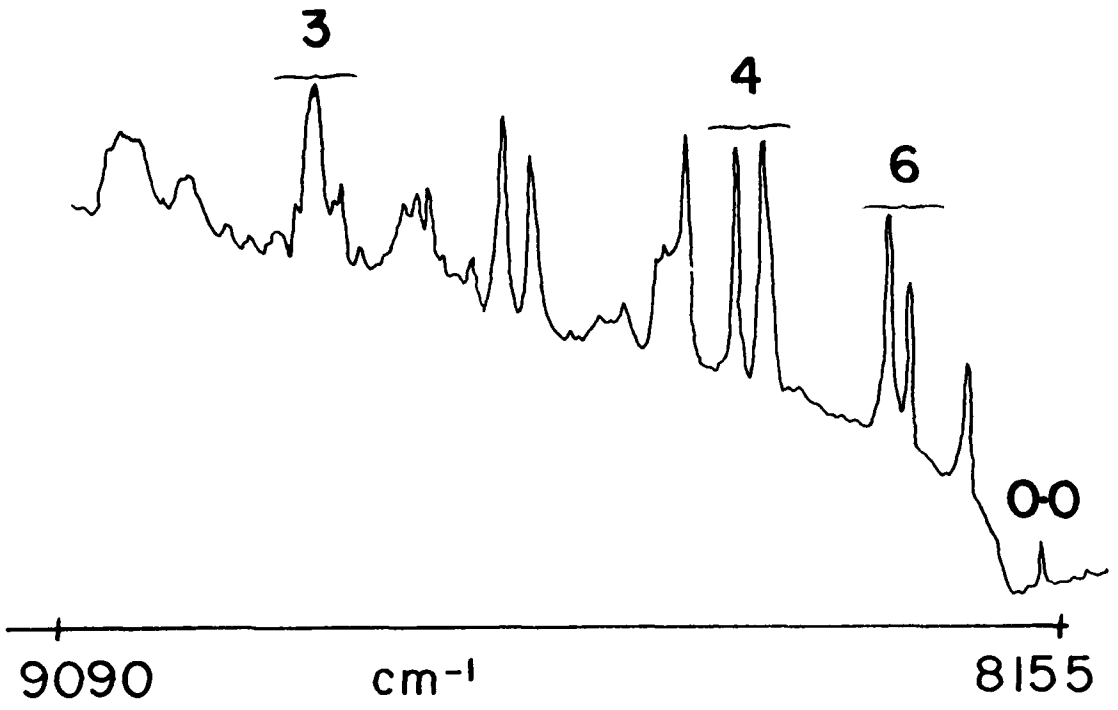

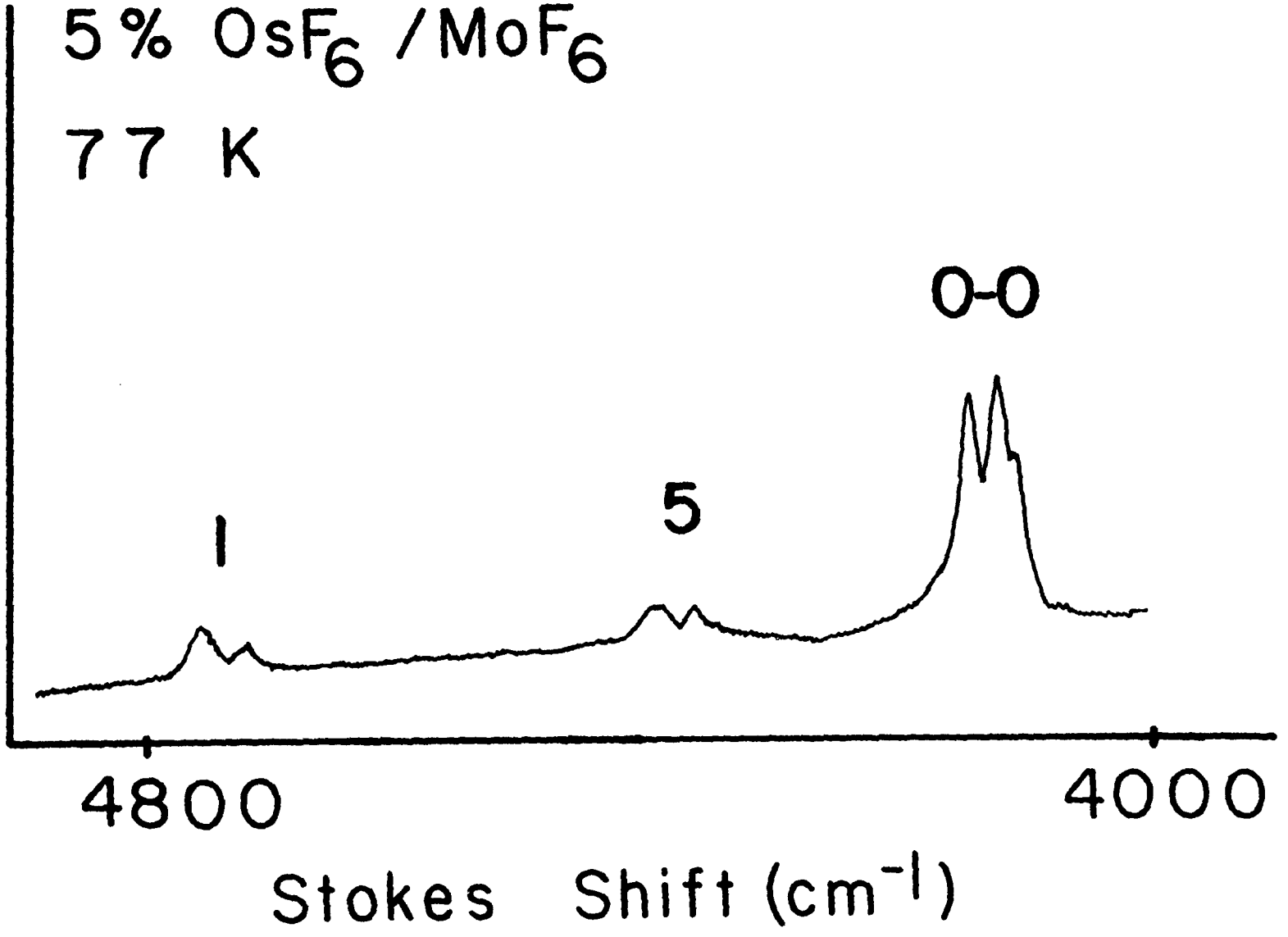
5% OsF_6 / MoF_6
77 K
0-0
5
1
4800
4000
Stokes Shift (cm^{-1})

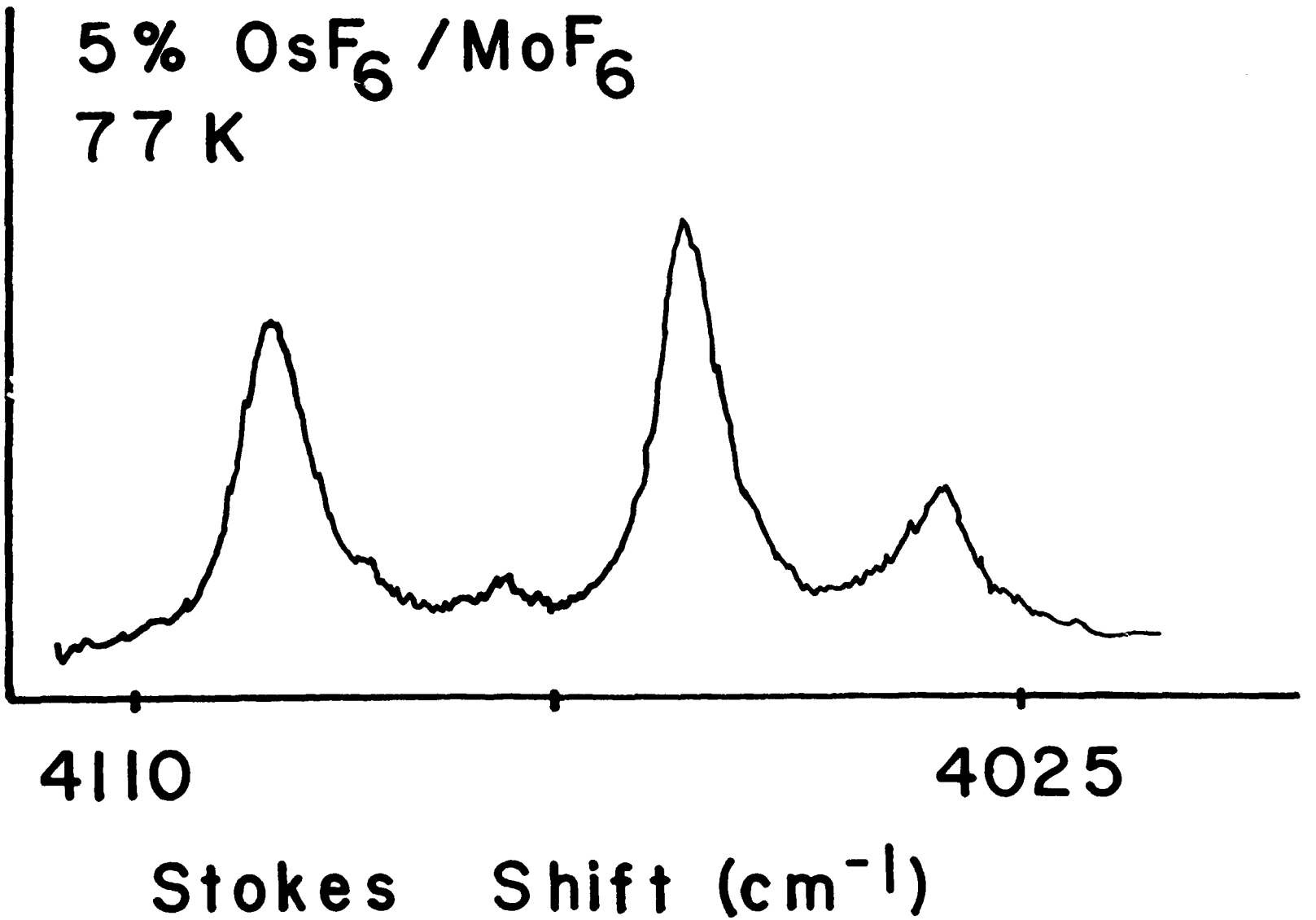
5% OsF_6 / MoF_6
77 K
4110
4025
Stokes Shift (cm^{-1})

SP482-3/A23

472:GAN:716:ddc
78u472-608

TECHNICAL REPORT DISTRIBUTION LIST, 051A

	No. Copies
Dr. M. A. El-Sayed Department of Chemistry University of California, Los Angeles Los Angeles, California 90024	1
Dr. C. A. Heller Naval Weapons Center Code 6059 China Lake, California 93555	1
Dr. J. R. MacDonald Chemistry Division Naval Research Laboratory Code 6110 Washington, D.C. 20375	1
Dr. G. B. Schuster Chemistry Department University of Illinois Urbana, Illinois 61801	1
Dr. A. Adamson Department of Chemistry University of Southern California Los Angeles, California 90007	1
Dr. M. S. Wrighton Department of Chemistry Massachusetts Institute of Technology Cambridge, Massachusetts 02139	1
Dr. M. Rauhut Chemical Research Division American Cyanamid Company Bound Brook, New Jersey 08805	1
Dr. J. I. Zink Department of Chemistry University of California, Los Angeles Los Angeles, California 90024	1
Dr. D. Haarer IBM San Jose Research Center 5600 Cottle Road San Jose, California 95143	1
Dr. John Cooper Code 6130 Naval Research Laboratory Washington, D.C. 20375	1
Dr. William M. Jackson Department of Chemistry Howard University Washington, DC 20059	1
Dr. George E. Walraffen Department of Chemistry Howard University Washington, DC 20059	1

TECHNICAL REPORT DISTRIBUTION LIST, GEN

	No. Copies
Mr. James Kelley DTNSRDC Code 2803 Annapolis, Maryland 21402	1
Mr. A. M. Anzalone Administrative Librarian PLASTEC/ARRADCOM Bldg 3401 Dover, New Jersey 07801	1

SP472-3/A1

472:GAN:716:enj
78u472-608

TECHNICAL REPORT DISTRIBUTION LIST, GEN

	No. Copies
Office of Naval Research Attn: Code 472 800 North Quincy Street Arlington, Virginia 22217	2
ONR Western Regional Office Attn: Dr. R. J. Marcus 1030 East Green Street Pasadena, California 91106	1
ONR Eastern Regional Office Attn: Dr. L. H. Peebles Building 114, Section D 666 Summer Street Boston, Massachusetts 02210	1
Director, Naval Research Laboratory Attn: Code 6100 Washington, D.C. 20390	1
The Assistant Secretary of the Navy (RE&S) Department of the Navy Room 4E736, Pentagon Washington, D.C. 20350	1
Commander, Naval Air Systems Command Attn: Code 310C (H. Rosenwasser) Department of the Navy Washington, D.C. 20360	1
Defense Technical Information Center Building 5, Cameron Station Alexandria, Virginia 22314	12
Dr. Fred Saalfeld Chemistry Division, Code 6100 Naval Research Laboratory Washington, D.C. 20375	1
U.S. Army Research Office Attn: CRD-AA-IP P.O. Box 1211 Research Triangle Park, N.C. 27709	1
Naval Ocean Systems Center Attn: Mr. Joe McCartney San Diego, California 92152	1
Naval Weapons Center Attn: Dr. A. B. Amster, Chemistry Division China Lake, California 93555	1
Naval Civil Engineering Laboratory Attn: Dr. R. W. Drisko Port Hueneme, California 93401	1
Department of Physics & Chemistry Naval Postgraduate School Monterey, California 93940	1
Scientific Advisor Commandant of the Marine Corps (Code RD-1) Washington, D.C. 20380	1
Naval Ship Research and Development Center Attn: Dr. G. Bosmajian, Applied Chemistry Division Annapolis, Maryland 21401	1
Naval Ocean Systems Center Attn: Dr. S. Yamamoto, Marine Sciences Division San Diego, California 91232	1
Mr. John Boyle Materials Branch Naval Ship Engineering Center Philadelphia, Pennsylvania 19112	1


DAT
ILM